Santeri Lappalainen

Suspension Arms' Flexibility and Impact in a Full Formula Student Vehicle Model

Metropolia University of Applied Sciences

Bachelor of Engineering

Automotive Engineering

Bachelor's Thesis

20 December 2023

Abstract

Author:	Santeri Lappalainen
Title:	Suspension Arms' Flexibility and Impact in a Full Formula Student Vehicle Model
Number of Pages:	60 pages + 6 appendices
Date:	20 December 2023
Degree:	Bachelor of Engineering
Degree Programme:	Automotive Engineering
Professional Major:	Automotive Design
Supervisor:	Pasi Oikarinen, Principal Lecturer

This thesis introduces a full vehicle simulation model and analyses simulation results from static and dynamic simulations between rigid and flexible lower suspension a-arms. The thesis underlays theory and measurements related to understanding the simulation model's functionalities and simulated results.

The simulation model was created with Adams Car and flexibility with Adams ViewFlex. The results were examined from the perspective of vehicle dynamics and impacts to its various subjects are explained

Results of this thesis include a full vehicle model of Metropolia Motorsport's season 2022-2023 Formula Student vehicle and a comprehensive analysis regarding the impact of flexibility. The model can be used to develop and explain future design and design decisions. The model can be modified for future revisions and developments.

Keywords: Formula Student, multibody simulation, vehicle dynamics, MSC Adams

---

Tiivistelmä

Tekijä:	Santeri Lappalainen
Otsikko:	Elastisten alustatukivarsien vaikutus Formula Student -auton simulaatiomallissa
Sivumäärä:	60 sivua + 6 liitettä
Aika:	20.12.2023
Tutkinto:	Insinööri (AMK)
Tutkinto-ohjelma:	Ajoneuvotekniikka
Ammatillinen pääaine:	Ajoneuvosuunnittelu
Ohjaaja:	Pasi Oikarinen, Lehtori

Tämä opinnäytetyö esittelee koko ajoneuvon simulaatiomallin ja analysoi saatuja tuloksia staattisista ja dynaamisista simulaatioista jäykkien ja elastisten alatukivarsien välillä. Työ pohjustaa tarvittavan teorian ja tehdyt mittaukset, joiden avulla simulaatiomallin toimintaa ja tuloksia pystytään ymmärtämään.

Simulaatiomalli luotiin Adams Car -ohjelmalla ja elastisuus ViewFlex -moduulilla. Tuloksia tutkittiin ajoneuvodynamiikan näkökulmasta ja vaikutukset siihen liittyviin käsitteisiin perusteltiin.

Tämän työn tuloksena syntyi koko ajoneuvon simulaatiomalli Metropolia Motorsportin kauden 2022-2023 Formula Student -kilpa-autosta ja laaja analyysi elastisuuden vaikutuksista. Mallia voidaan käyttää tiimin sisällä jatkokehityksessä ja tulevaisuuden designeissa sekä niihin liittyvissä päätöksissä. Malli on muokattavissa ja kehitettävissä tulevaisuuden revisioita varten.

Avainsanat: Formula Student, multibody-simulaatio, ajoneuvodynamiikka, MSC Adams

Contents

List of Abbreviations

HPF023:	Metropolia Motorsport’s season 2022-2023 Formula Student Vehicle
FS:	Formula Student
EV:	Electric Vehicle
CV:	Combustion Vehicle
DOF:	Degree of Freedom
TIRF:	Calspan Tire Research Facility
FSAE TTC:	The FSAE Tire Test Consortium
COG:	Center of Gravity
FSG:	Formula Student Germany
MNF:	Modal Neutral File
FEA:	Finite Element Analysis
IMU:	Inertia Measurement Unit

1 Introduction

In this thesis a functioning multibody simulation model based on Metropolia Motorsport's 2022-2023 season Formula Student vehicle HPF023 was built. Various driving conditions were simulated with the simulation model with flexible and rigid suspension arms. The target was to obtain realistic results from the simulations compared to the actual vehicle's driving data and examine the impact of flexibility from the perspective of vehicle dynamics.

Based on the simulation results, more advanced analyses were made from different aspects of vehicle dynamics in a function of force affecting in suspension arms, between the tires and monocoque chassis.

This thesis requires basic knowledge of vehicle dynamics including tires and basic operations as well as skills with MSC Adams from its reader. The purpose of this thesis is not to be educational material regarding the topics above.

1.1 Formula Student

Formula Student is an international engineering design competition for students from universities globally. The target is to build a rule compliant Formula Student vehicle and compete with it in Formula Student competitions around the world. Most well-known competitions are held in various countries in Europe and North-America. The vehicles compete in combustion, electric and driverless categories. The competitions are divided to static and dynamic events. The static events consist of: Engineering Design, Cost Event, and Business Plan Presentation. The dynamic events consist of: Acceleration, Skidpad, Autocross, Endurance, and Efficiency. Static events are evaluated by judges and points from dynamic events are given based on time.

1.2 Metropolia Motorsport and HPF023

Metropolia Motorsport is the first and only Finnish Formula Student team competing in the category of electric vehicles (EV). The team was founded in 2000 and attended its first competitions in season 2002-2003. During the season 2012-2013 the team transferred from the category of combustion vehicles (CV) to EV category.

HPF023, which can be seen in a figure 1, is the team's 9th vehicle in EV category and 19th vehicle that has attended competitions. It is the team's first vehicle with monocoque chassis which is made of carbon fibre, and first vehicle with decoupled suspension separated to heave and roll elements. HPF023 is also the team's second configuration of 4WD FS-vehicle, and it has carbon fibre suspension arms, 10" wheels, 600 V accumulator, inverters from Lenze which operate separately with front and rear motors from Fischer and aero package including front and rear wing, side wings and diffuser.

Figure 1. HPF023 on track.

1.3 Thesis Goals

The main goals of this thesis were to build a functioning multibody simulation model based on HPF023 using software MSC Adams and to compare the impact of flexible and rigid suspension arms. Flexibility to suspension arms was created with Adams ViewFlex and the simulation model itself was built and analysed with Adams Car.

Learning to operate fluently with MSC Adams was also highlighted and one of the desired results of this thesis was to create a full vehicle model which can be used in future design events as a basis for design decisions made by the team or subsystems and is easily modified for the future implementations.

Understanding received results from the simulation model in different conditions from the view of vehicle dynamics and comparing the results to the data gained from the track. Assimilate and understand the impact of several factors related to vehicle dynamics and being able to explain the difference caused by the flexibility.

2 Theory

2.1 Tires

A vehicle is attached to the ground with a contact patch of tires. The contact patch of the tire needs to produce forces in every driving circumstance to maintain the control and stability of the vehicle. Consequently, tire behaviour is defined with its ability to produce forces and torques. When discussing racing vehicles, it is desirable to maximize acceleration in all driving conditions.

Longitudinal force is produced when torque is applied to the wheel by the powertrain or brakes. Lateral force is produced when the direction of the tire is deflected from its original direction. The angle between these directions is called slip angle which can be seen from the figure 2. The slip angle of a tire enables a vehicle to change direction when steering input is applied.

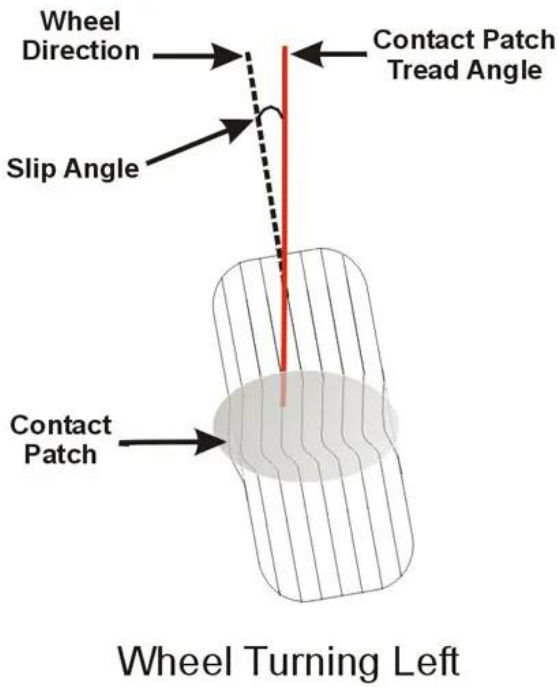

Figure 2. Slip angle of a tire. [1]

Tire behaviour regarding force production can be observed with a friction ellipse. The ellipse diagram shows the tire's ability to produce longitudinal force in X-axis

and lateral force in Y-axis with different inclination angles and normal loads. Figure 3 shows that when the tire acquires peak lateral force values, the production of longitudinal force is decreasing near to zero. The same applies also when the tire acquires peak longitudinal force values. This means that a tire is not able to produce maximum values of both forces at the same time. A tire produces maximum lateral force in pure lateral acceleration (cornering) and maximum longitudinal force in pure longitudinal acceleration or deacceleration (braking). Between maximum values there occurs force production of both directions, for example when the vehicle is entering to a corner. Hence it can be deduced that the greater the friction ellipse, the better the tire performance. [2, p. 57-61]

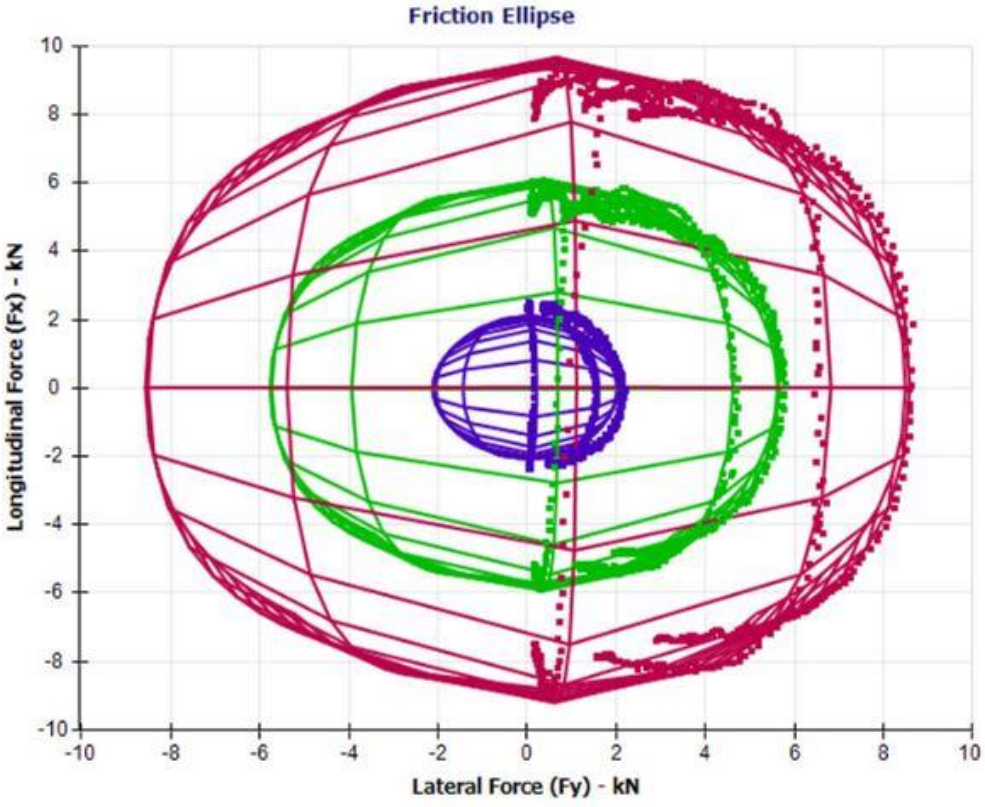

Figure 3. Example of friction ellipse. Colours are presenting vertical forces. [3]

2.1.1 Tire Testing and Data

In general, tires can be tested with different machines and methods. In this thesis the focus is on Formula Student tires. Tire tests to FS-tires are completed in Calspan Tire Research Facility (TIRF), which is located in the United States of America. An organization called The FSAE Tire Test Consortium (FSAE TTC) provides tires and wheels to TIRF and maintains a private server, where they deliver testing data. The organization is managed by volunteers, and schools pay 500 $ to gain access to the server.

Tires at TIRF are tested in different rounds. Each round consists of tires tested with different compounds, sizes and wheels. Until present, TIRF has provided nine testing rounds with a total amount of 48 different tire-wheel combinations.

The tire testing is completed with several sweeps on a flat-belt tire test machine. Nominal velocity of the flat-belt is 11.176 m/s. Data is collected with a frequency between 10-100 Hz. The test output channels are: Elapsed Time, Road Velocity, Slip Angle, Inclination Angle, Slip Ratio, Normal Load, Lateral Force, Longitudinal Force, Aligning Torque, Overturning Moment, Loaded Radius, Effective Radius, Wheel RPM, Tire Pressure, Tire Surface, Ambient Temperature, and Road Surface Temperature. Tires are tested and strained with different loads, nominal pressures et cetera, depending on the type of test sweep. Tire testing of motorsport tire can be seen from the following figure 4.

Figure 4. Tire testing at Calspan. [4]

2.1.2 Tire Models

Tires can be observed with a variation of different factors. These factors are divided to primary task functions and secondary effects. When studying further, the functions and effects are separated to categories under steady state and vibratory behaviour. [5, p. 59-61]

The concept of tire model is considered as a mathematical model. Models can be categorised based on their purpose. There are commonly four different ways or categories to approach the development of a tire model: from experimental data only, using the similarity method, through simple physical model as well as through complex physical model. These categories can be positioned to a diagram which describes their qualities. The categories are sectioned more empirical to the left and more theoretical to the right. The diagram, principles for the category division and more detailed explanations regarding the categories are illustrated in figure 5.

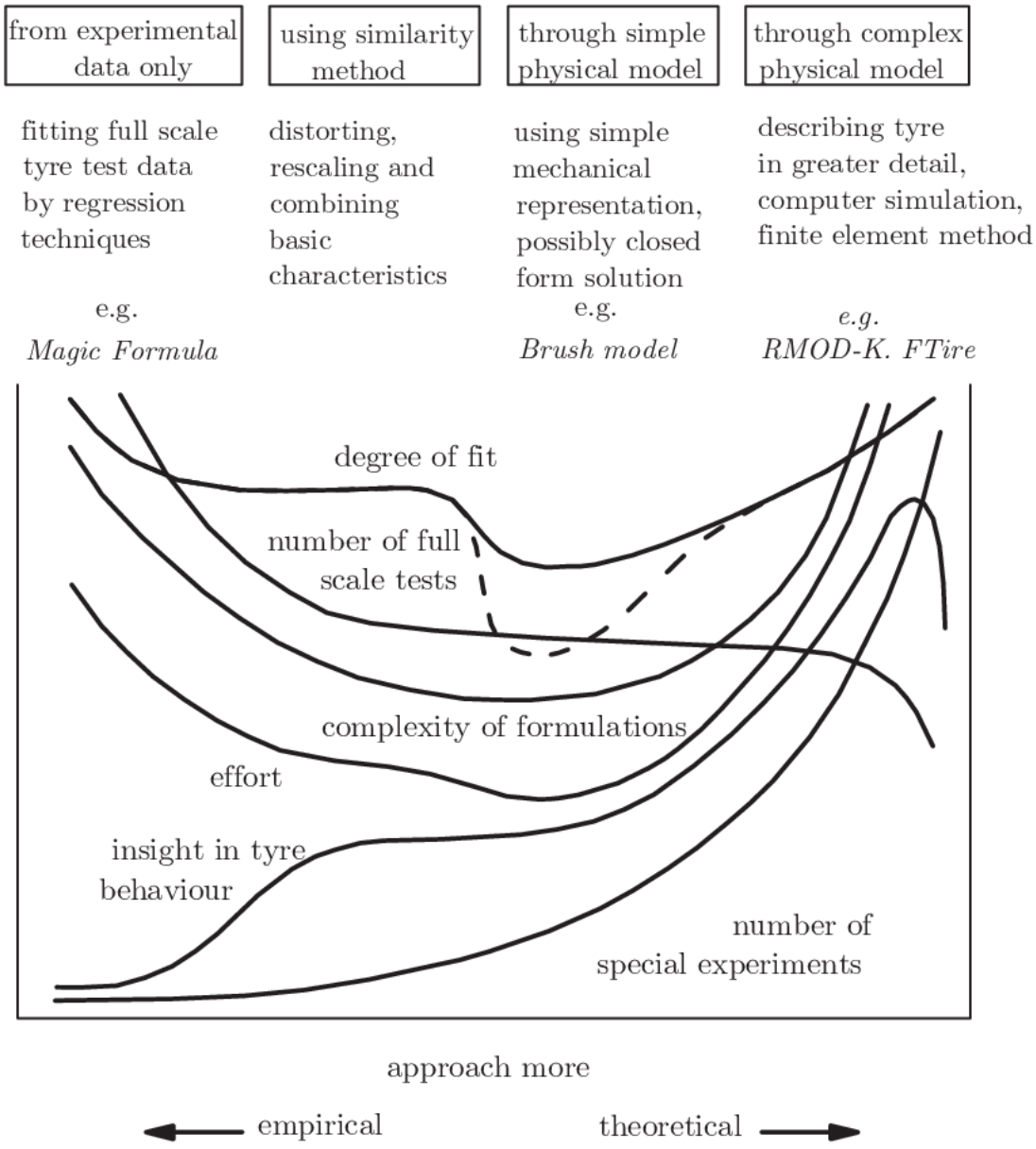

Figure 5. Illustration of tire model approaches. [5, p. 81]

More empirical or semi-empirical tire models are typically used in vehicle motion simulations because they are less complex. The similarity method observes that when a tire is running in conditions differing from the reference conditions, pure slip curves remain similar in shape. The reference condition is defined with nominal load at camber equals to zero as well as free rolling or side slip angle on a given road surface. Pure slip conditions reference curves are defined with different functions [5, p. 150]. The reference function of lateral force is given in following equation [5, p. 152]:

$$F_y = \frac{F_z}{F_{zo}} * F_{yo} * (\alpha_{eq}) \tag{2.1}$$

where F_y is the lateral force reference, F_z is the wheel load, $F_{zo}$is the nominal load, F_{yo} is the reference lateral force with the subscript o, and α_{eq} is the equivalent slip angle. The equivalent slip angle can be defined with the following equation [5, p. 152]:

$$\alpha_{eq} = \frac{F_{zo}}{F_z} * \alpha \tag{2.2}$$

where α is slip angle. Derivative of lateral force with respect to slip angle when $\alpha = 0$ gives same value for the slope than derivative of lateral force reference with respect to equivalent slip angle when $\alpha_{eq} = 0$ which is equal to original cornering stiffness. This can be seen from the following equation [5, p. 152]:

$$\frac{\partial F_y}{\partial \alpha} = \frac{F_z}{F_{zo}} * \frac{dF_{yo}}{d\alpha_{eq}} * \frac{\partial \alpha_{eq}}{\partial \alpha} = \frac{dF_{yo}}{d\alpha_{eq}} = C_{F\alpha o} \tag{2.3}$$

where $C_{F\alpha o}$ is the original cornering stiffness. Aligning torque and its characteristics are also included to the new condition of reference function. Similar concept with the same equivalent slip angle can be seen in the following equation [5, p. 153]:

$$M_z = \frac{F_z}{F_{zo}} * \frac{C_{M\alpha *(F_z)}}{C_{M\alpha o}} * \frac{C_{F\alpha o}}{C_{F\alpha *(F_z)}} * M_{zo} * (\alpha_{eq}) \tag{2.4}$$

where M_z is the aligning torque, $C_{M\alpha}$ is the aligning stiffness, $C_{M\alpha o}$ is the reference aligning stiffness, $C_{F\alpha}$ is the reference for cornering stiffness and M_{zo} is the reference for aligning torque.

Reference characteristics can be also described by using a base function of magic formula tire model. There are several equations to define the different factors to the main function. The function and magic formula tire model are being explained in the following chapter.

2.1.3 Pacejka's Magic Formula Tire Model

The tire model called Pacejka's Magic Formula is a Semi-Empirical Tire Model for calculating steady-state tire force and moment characteristics. The main purpose of Semi-Empirical Tire Models is to be used in vehicle simulation environment. They may contain structures from physical tire models but are mainly based on measured data. The Magic Formula is based on the following equations:

$$y = D * \sin\left(C * \tan^{-1}(B * x - E * (B * x - \tan^{-1} B * x))\right) \quad (2.5)$$

$$Y(X) = y(x) + S_V \quad (2.6)$$

$$x = X + S_H \quad (2.7)$$

where Y or y is the output variable which is lateral force, longitudinal force or aligning torque, X or x is the slip parameter (slip angle or longitudinal slip), B is the stiffness factor, C is the shape factor, D is the peak value, E is the curvature factor, S_V is the vertical shift and S_H is the horizontal shift [5, p. 165].

The functions above draw a curve where factors B, C, D and E define characteristics to the slope and shifts S_V and S_H allow the curve to have an offset with respect to the origin [5, p. 166]. The impact of every factor can be seen in the figure 6. Factor parameters are measured data from tire testing and calculated with different equations and with different input variables which are briefly explained in the following paragraph.

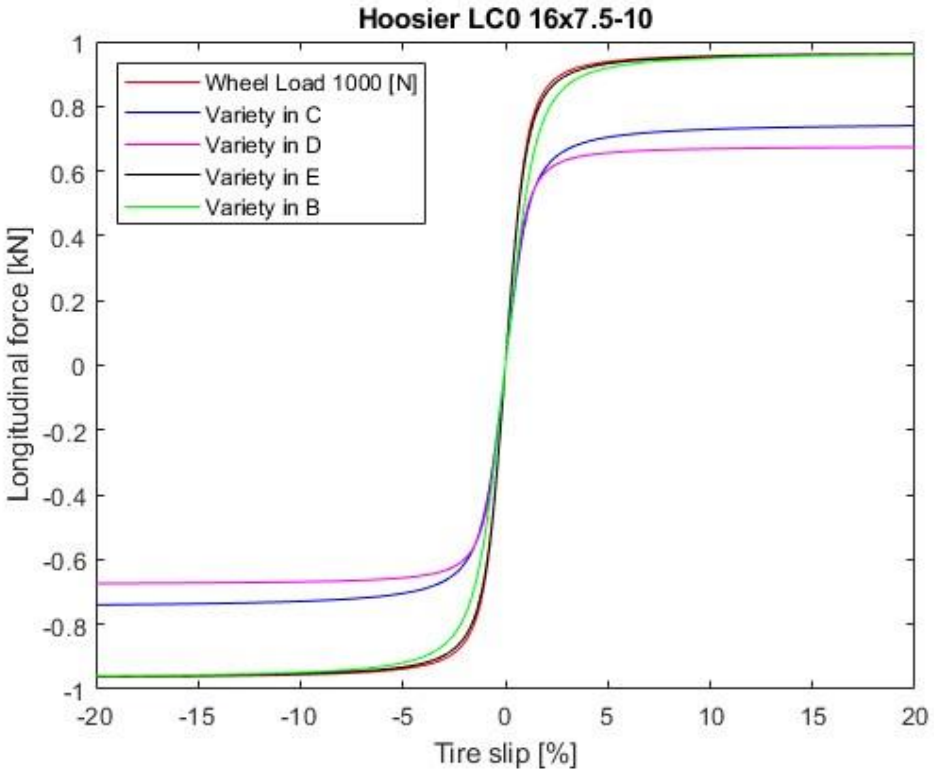

Figure 6. Longitudinal force production of Hoosier LC0 tire and impacts of different factor values to the curve.

The red curve in the figure above shows the longitudinal force production LC0 tire with 1000 N wheel load. The appointed factor in the other curves is deviated 0.3 from its initial value with 1000 N wheel load to only illustrate its impact to characteristics of the curve. In reality, the values for the factors are not existing with the given wheel load.

The shape factors and shifts to longitudinal force with pure longitudinal slip which means that slip angle of the tire equals zero and can be calculated with the following equations [5, p. 179]:

$$B_x = \frac{K_{x\kappa}}{(C_x * D_x + \varepsilon_x)} \tag{2.8}$$

where K_{xk} is the brake slip stiffness and ε_x is the reduction factor.

$$C_x = p_{Cx1} * \lambda_{Cx} \tag{2.9}$$

where p_{Cx1} is the shape factor for longitudinal force and λ_{Cx} is the scaling factor for p_{Cx1}.

$$D_x = \mu_x * F_z * \zeta_1 \tag{2.10}$$

where μ_x is the peak friction coefficient, F_z is the wheel load and ζ_1 is an additional factor for normally encountered conditions.

$$E_x = (p_{Ex1} + p_{Ex2} * df_z + p_{Ex3} df_z^2) * \left(1 - p_{Ex4} * sgn(\kappa_x)\right) * \lambda_{Ex} \quad (\leq 1) \tag{2.11}$$

where p_{Ex1} is the longitudinal curvature at nominal vertical load, p_{Ex2} is the variation of curvature with load, f_z is the vertical force, p_{Ex3} is the variation of curvature with load squared, p_{Ex4} is the factor in curvature while driving, $sgn(\kappa_x)$ is the sign of abscissa in the function of longitudinal slip and λ_{Ex} is the scaling curvature factor.

$$S_{Vx} = (F_z * (p_{Vx1} + p_{Vx2} * df_z) * \lambda_{Vx} * \lambda'_{\mu x} * \zeta_1 \tag{2.12}$$

where p_{Vx1} is the vertical shift at nominal wheel load, p_{Vx2} is the variation of vertical shift with load, λ_{Vx} is the vertical shift scaling factor and $\lambda_{\mu x}$ is the peak friction coefficient scaling factor.

$$S_{Hx} = (p_{H1x} + p_{H2x} * df_z) * \lambda_{Hx} \tag{2.13}$$

where p_{H1x} is the horizontal shift at nominal wheel load, p_{H2x} is the variation of horizontal shift with load and λ_{Hx} is the horizontal shift scaling factor.

Similar equations are used when factors and shifts are calculated for lateral force with pure side slip, which means that the longitudinal slip of the tire equals zero, aligning torque with pure side slip and for combinations where combined slip occurs.

Several versions of the Magic Formula model exist. The model has developed while technology and knowledge have evolved. Frequency in various driving conditions for the data collection from tire testing has risen up to 100 Hz. Combining slip in the steady-state conditions and implementing inflation pressure effect has also become possible. PAC2002 tire model was decided to be used in the simulation model of this thesis. PAC2002 is meant to be used in simulations where the road is assumed to be smooth and more or less flat. Other major reason was the software. PAC2002 is licensed by MSC software which is the provider of MSC Adams [6]. In conditions where the road is assumed to be more or less rough and bumpy, another tire model would be used.

2.2 Vehicle Dynamics

Vehicle dynamics covers a vehicle's behaviour and motions in different driving conditions as well as interactions with driver. Behaviour and motions can be examined in translational envelopes which are longitudinal (X), lateral (Y) and vertical (Z), and in rotational envelopes which are roll (around X), pitch (around Y) and yaw (around Z). These envelopes are commonly called 6-DOF and can be seen in figure 7.

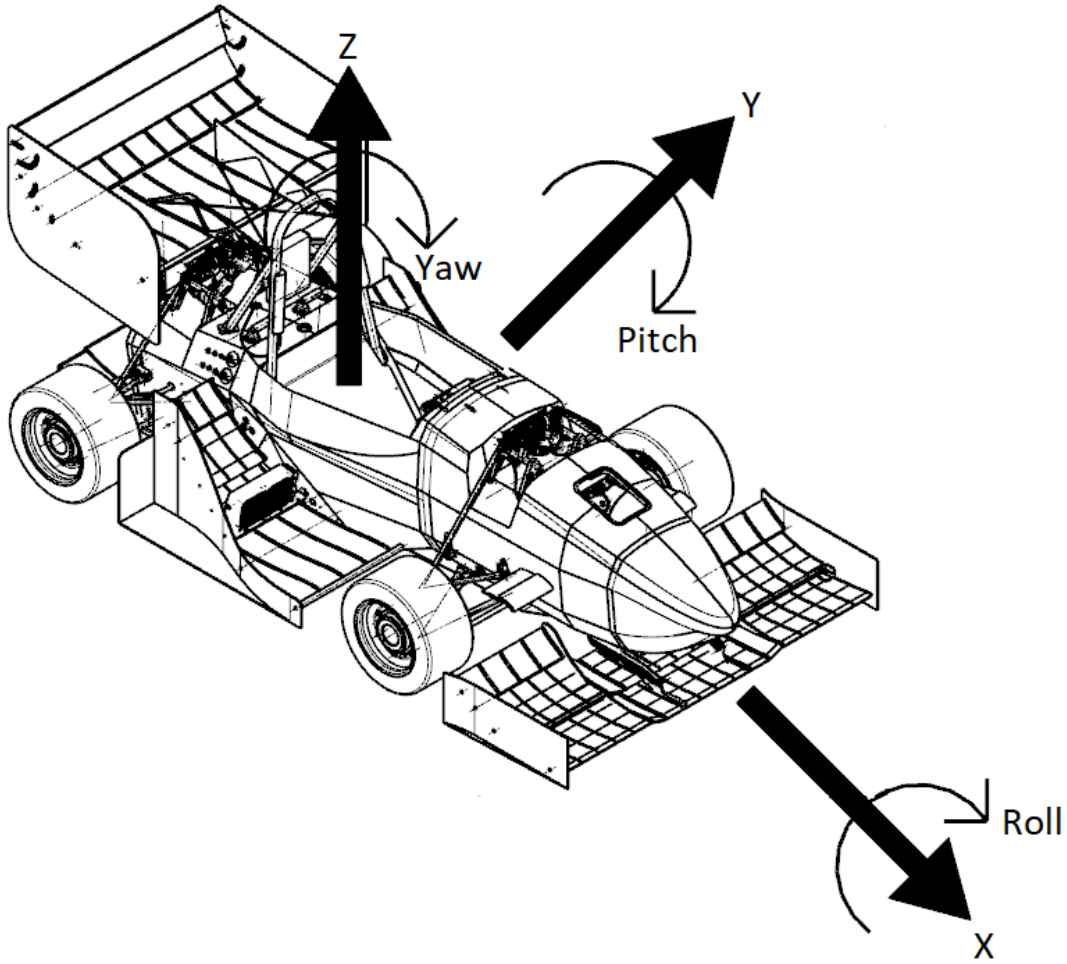

Figure 7. 6-DOF illustrated.

Suspension and steering, aerodynamics, tires, powertrain, brakes and mass distribution are the mutual factors affecting the vehicle dynamics. The vehicle gets its motion by the force coming from or produced by the powertrain. The force is then applied to the road from the tires. Several driving resistances are resisting the vehicle's motion, and the vehicle's state of motion depends on the relation between these which can be seen in the following equation [7]:

$$F_k = \Sigma F_W \tag{2.14}$$

where F_k is the force moving the vehicle and ΣF_W are the forces resisting the motion. ΣF_W is a sum of forces which is normally consisting of rolling resistance, air resistance and slope resistance.

In racing vehicles and motorsports, maximizing the friction force generated between the tire and road surface in every driving condition is required. This force is also known as grip and can be calculated with the following equation:

$$F_{\mu} = \mu * N \tag{2.15}$$

where F_{μ} is the friction force, μ is the friction coefficient and N is the normal force.

2.2.1 Suspension Kinematics

The geometry of a vehicle's suspension is the best compromise of several constructs depending on the vehicle's use. The initial subject of examination is suspension type, which defines the constructs of suspension. HPF023 uses double a-arm or double wishbone suspension and consequently all the constructs in this thesis are observed like they exist in a double a-arm suspension.

The angle of the tire to its vertical axis from the front view is called camber. Camber is negative when the wheels are horizontally pointing towards the vehicle and positive when they are pointing outwards from the vehicle. Vehicle's camber gain means the change in camber angle when the wheel is vertically displaced and it defines the amount of static camber is being set to the vehicle. Negative camber is commonly used in racing vehicles. When a vehicle is cornering and encounters body roll, lateral wheel load transfer is directed to the outside wheel. Therefore, when the wheel has negative camber, its inner contact patch rises and enables the tire to have the entire contact patch in contact with the road. In motorsport, it is desired to have a maximum contact patch in contact with the road, hence when the outer wheel gains positive camber in dynamic conditions, it is desirable to set a matching amount of static negative camber to the wheel.

The angle of the tire to its longitudinal axis from the upper view is called toe. A vehicle has *toe in* when the front edges of the wheels point towards the vehicle and *toe out* when the front edges are pointing outwards from the vehicle. Toe in

increases the vehicle's stability when driving straight line in both axles. Toe out instead decreases the vehicle's straight-line stability but increases the vehicle's reactions for turning when steering input is applied. In the rear axle toe out may cause oversteering.

Caster angle is the angle between the wheel's vertical axis and king pin axis which strikes through the ball joints of the upper and lower a-arms from the side view. The caster of HPF023 can be seen from figure 8.

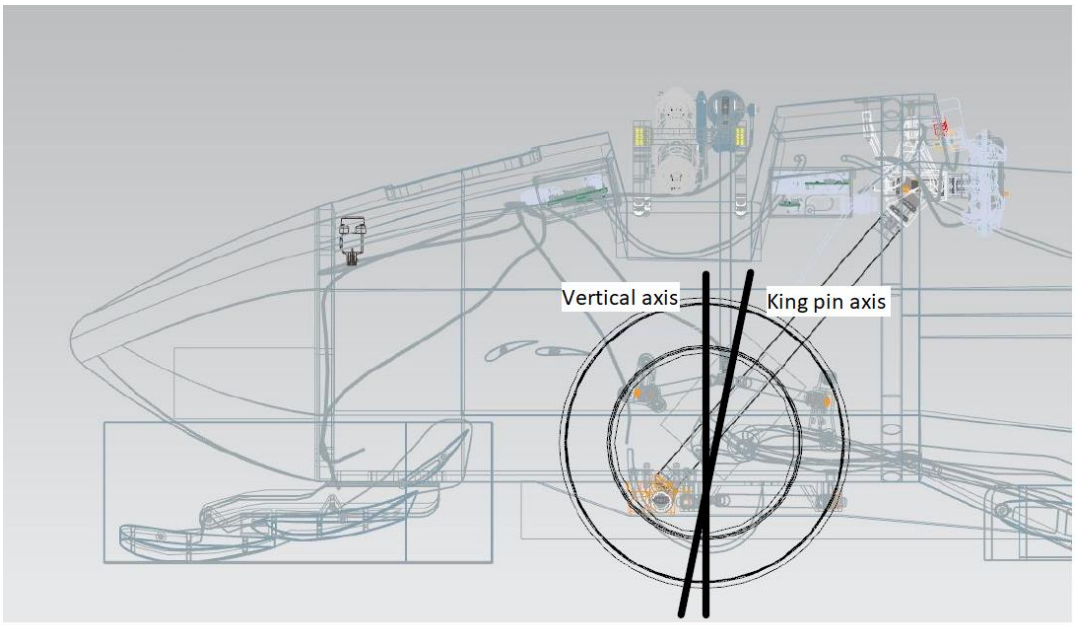

Figure 8. Caster of HPF023.

Caster is positive when the top mount of the king pin axis is located more rearward than the lower mount of the king pin axis. The main advantages of positive caster are its ability to create self-aligning torque and the ability to have camber gain when cornering. Self-aligning torque pulls the wheels back straight and makes the vehicle more stable but it also requires more steering input from the driver.

Similar to caster, king pin inclination is the angle between the wheel's vertical axis and king pin axis but from the front view. King pin inclination creates vertical

displacement of the vehicle during a steering maneuver. The distance between these axes when they touch the ground is called scrub radius. Positive scrub radius enables the wheel to roll over on lock [8]. The king pin inclination and positive scrub radius of HPF023 can be seen from the following figure 9.

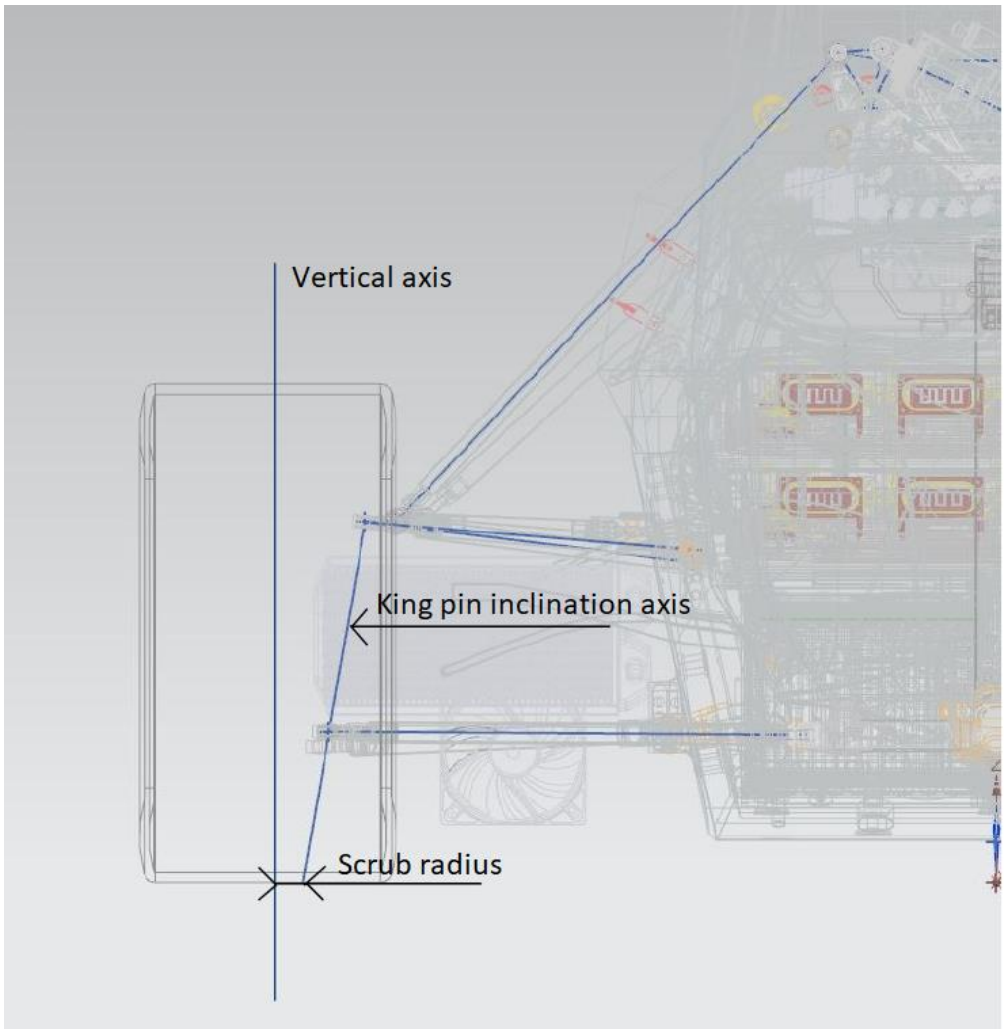

Figure 9. Illustration of king pin inclination axis and scrub radius.

If both wheels are turning the same amount during steering, the steering is called parallel steering. When the wheels are turning nonparallel, the steering geometry is called Ackermann. In Ackermann steering geometry, the inside wheel of the vehicle is turning more than the outside wheel. In anti-Ackermann, the outside wheel is turning more than the inside wheel.

Vehicle can also have anti-geometries which are usually recognized as anti-squat, anti-dive and anti-lift. 100 % of any anti-geometry means that none of the attributes caused by anti-geometry occurs. Anti-squat affects the rear axis of the vehicle and means that during an acceleration, an affecting force compresses the rear suspension of the vehicle towards the ground. This occurs when the percentage is below 100 %. Anti-dive affects the front axis of the vehicle and means that during braking the affecting force compresses the front suspension of the vehicle towards the ground. This occurs when the percentage is below 100 %. Anti-lift means that the front wheels are rising and rear wheels are squatting during an acceleration. This is more typical with front and four-wheel drive vehicles. When 100% of anti-geometries is exceeded the behaviour of the vehicle becomes unexpected and the vehicle feels unpleasant to drive.

2.2.2 Dynamic Wheel Loads

A vehicle has its main dynamic wheel load transfer in longitudinal and lateral directions. Longitudinal load transfer occurs when the vehicle is accelerating or deaccelerating (braking). Force caused by longitudinal acceleration ("centrifugal force") is generated and occurs in the vehicle's center of gravity (COG) towards the front or rear depending on whether the vehicle is accelerating or braking. Reaction forces from the tires affect in the opposite direction. Longitudinal wheel load transfer can be calculated with the following equation [9, p. 83]:

$$\Delta W_x = \frac{h}{L} * W * A_x \tag{2.16}$$

where ΔW_x is the increased wheel load in rear when accelerating or increased wheel load in front when braking, h is the height of COG from the ground, L is the wheel base, W is the total mass of the vehicle and A_x is the longitudinal acceleration.

Lateral load transfer occurs when the vehicle is cornering. Force caused by lateral acceleration is generated and occurs in the vehicle's COG towards the left or right side of the vehicle, depending on which direction the vehicle is cornering.

Reaction forces from the tires affect in the opposite direction. Lateral wheel load transfer can be calculated with the following equation [9, p. 81]:

$$\Delta W_y = \frac{1}{2} * \frac{W * A_y * h_R}{t} \quad (2.17)$$

where ΔW_y is the increased wheel load in left or right wheel in a front or rear axle, W is the total mass of the vehicle, h_R is the distance between the COG and front or rear axle's roll center and t is the track width.

Vehicle handling characteristics are a sum of several factors. Suspension can be adjusted with springs and dampers between soft and stiff, which has a direct impact on the vehicle's behaviour. When the vehicle has softer front or stiffer rear, less amount of front wheel load transfer occurs and the front tires have more grip. This may result in the vehicle's oversteering, whereas a vehicle with stiffer front or softer rear causes more front wheel load transfer and, in that case, less grip on the front tires. This may result in the vehicle's understeering. Stiffness of the vehicle's body separates front and rear suspensions from each other. If the body is too soft compared to front and rear suspension stiffnesses, the balance between the front and rear becomes difficult to adjust.

Longitudinal and lateral accelerations also depend on several factors and affect the vehicle characteristics. Kinematics define positions of roll centers on front and rear axles. Front and rear of the vehicle roll around their roll centers. Roll axle is then an axle from the front roll center to the rear roll center. COG height from the ground and vertical distance between the COG and roll axle have a major impact on the vehicle's behaviour.

2.2.3 Aerodynamics

The purpose of aerodynamical devices is to channel the air flow and add downforce, which is also known as negative lift, to the vehicle. Increasing the downforce means increasement to vertical wheel loads. When the vehicle has

more wheel loads in dynamic conditions, tires need to produce more longitudinal and lateral forces. When there are more tire forces, the tires produce more grip.

Aerodynamical devices also increase drag, and the adequate ratio between lift and drag needs to be optimized. The aero balance, which is distribution of downforce through front and rear tires, has a major impact on the vehicle's behaviour. The distribution of aero balance needs to be taken into account when adjusting suspension and ride heights of the vehicle. Aerodynamic simulation of HPF023 can be seen from the following figure 10.

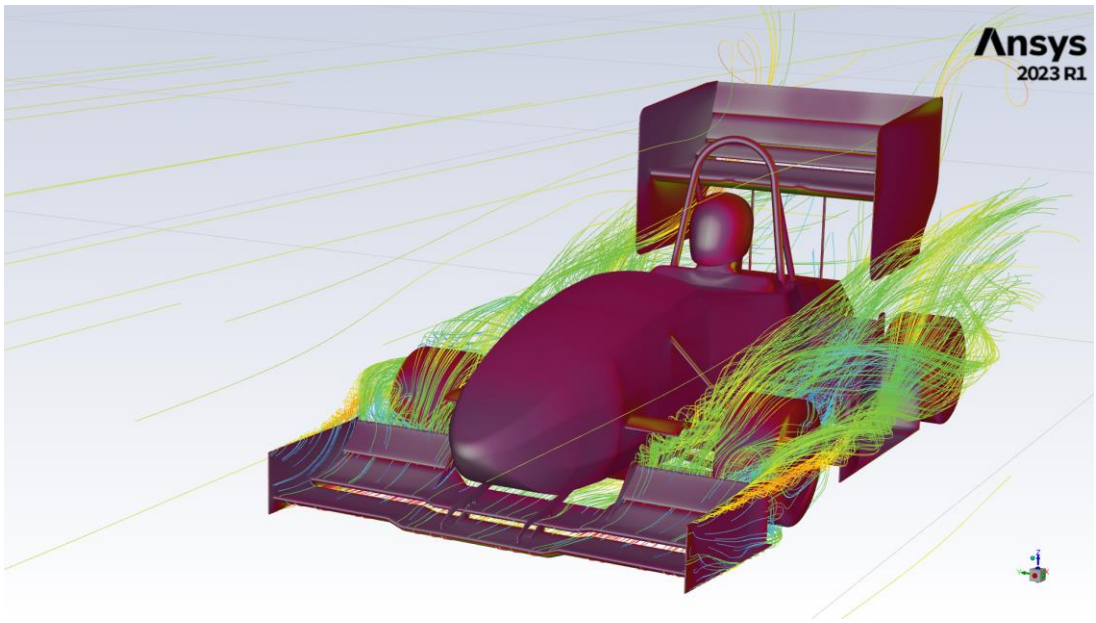

Figure 10. Aerodynamic simulation of HPF023.

2.3 HPF023's Measures

For the full vehicle simulation model, certain measurements were needed for building a model that corresponds with the actual vehicle. These measurements were used when creating mass and inertia properties for each part.

2.3.1 Center of Gravity

Measuring the location of HPF023's COG was started by weighing corner weights. When the vehicle was set on top of the corner scales, lateral and

longitudinal weight distributions were adjusted and balanced while maintaining the ground clearance of 35 mm for the whole vehicle. The measurement results can be seen from figure 11. Formula Student Germany (FSG) rules define minimum ground clearance of 30 mm [10, p. 26]. For this value, minor safety factor (+5 mm) was desired. Adjustments were made from pushrods' rod ends.

Figure 11. HPF023 corner weights with 85 kg driver.

After the corner weights were measured and adjusted, COG measuring was completed. For that, front axle's corner scales were placed on a 4-post car lift and rear scales were placed on the ground. HPF023 was placed on top of the scales and the car lift was initially raised 0.35 m from ground level. First weights were measured on that height. After that, the vehicle was raised with 0.05 m steps from the initial height to 0.7 m and then back to the initial height with the same steps. HPF023 in the highest position (0.7 m from ground level) can be seen in the figure 12. Weight measures were taken from every step.

Figure 12. HPF023 during COG measurements.

When the measuring was completed, calculations for COG's longitudinal position (X) and COG's vertical position from the ground (Z) were made. Longitudinal position of COG was calculated with the following equation [9, p. 82]:

$$a = \frac{F_R * L}{G} \tag{2.18}$$

where a is the COG's distance from the front axle, F_R is the rear weight of the vehicle, L is the wheelbase and G is the total weight of the vehicle.

Vertical position of the COG from the ground was calculated with the following equations [9, p. 82]:

$$\theta = sin^{-1} * \frac{B}{L} \tag{2.19}$$

where θ is the angle of elevation and B is the lifted height.

$$c = R_d * tan\theta \tag{2.20}$$

where c is the changing variable (hypotenuse) with the angle of elevation and R_d is the tire radius.

$$h = \frac{-cos\theta*(G*(a-c)-F'_R*L)}{sin\theta*G} \tag{2.21}$$

where F'_R is the measured rear weight when front of the vehicle is lifted and h is the COG's vertical distance from the ground. COG height from the ground was calculated to all the steps mention above. The final vertical height of the COG was then calculated by calculating the average from the COG height results.

2.3.2 Unsprung Mass

Mass of unsprung parts were measured with a precision scale which can be seen from figure 13. Generally, for vehicles two of a one third of the weight of suspension arms is defined as an unsprung mass.

Figure 13. HPF023's wheel on the precision scale.

2.3.3 Mass Moment of Inertia

Physical testing to measure mass moment of inertia of the vehicle was not possible because the lack of a necessary measuring device. A CAD software was used for evaluating inertia values. In CAD it was not possible to enter material properties for every part, hence the inertia values were evaluated with the heaviest parts of the vehicle assembly’s sprung mass.

2.4 Material Properties

Different materials behave in differently when an external stress is applied to them. Properties of certain material can be defined in several ways depending on

the situations where the material is being examined. Materials used in this thesis are elastic, which means that the material recovers to its original shape after it has been strained. The purpose is to examine and compare behaviour of the vehicle when the suspension arms are rigid and then set to have elastic properties.

Steel and carbon fibre are elastic materials and were used in the simulations. Elastic materials are divided into different types. Steel is elastic isotropic material which means it has the same properties in every direction. Carbon fibre can be defined as elastic anisotropic or elastic orthotropic material which means that its properties will vary in different directions. In Adams ViewFlex, the density of every material needs to be set. For isotropic materials, Youngs Modulus, which describes the stiffness of the material, and Poisson's Ratio, which describes the ratio between transverse contraction strain and longitudinal extension strain, need to be set. For anisotropic or orthotropic materials, Youngs modulus and Shear modulus, which describes a material's ability to resist deformation of shear, need to be set for different directions.

3 MSC Adams

MSC Adams is a software made for multibody dynamic simulations. There are several modules under Adams. All the simulations and models in this thesis were made with module Adams Car, which is made for modelling and simulating vehicles and analysing the results. Module Adams ViewFlex was used to create elasticity to suspension arms. ViewFlex creates a modal neutral file (MNF) for a specific part. MNF-file uses finite element analysis (FEA) to transform a rigid part to flexible part or body. After that, the flexible part can be imported to the Adams Car model.

3.1 Template

There are two modes in Adams Car. Template Builder is a mode where the user creates a topology for a model. The model's topology is called a template and can be, for example, front suspension or steering. The template is created in space, where Adams Car uses three-dimensional X, Y and Z -coordinate system, where X is the longitudinal direction, Y is the lateral direction and Z is the vertical direction. Positive X direction is pointing to the front of the vehicle, positive Y direction is pointing to the left side of the vehicle and positive Z direction is pointing to the top of the vehicle as seen in figure 14.

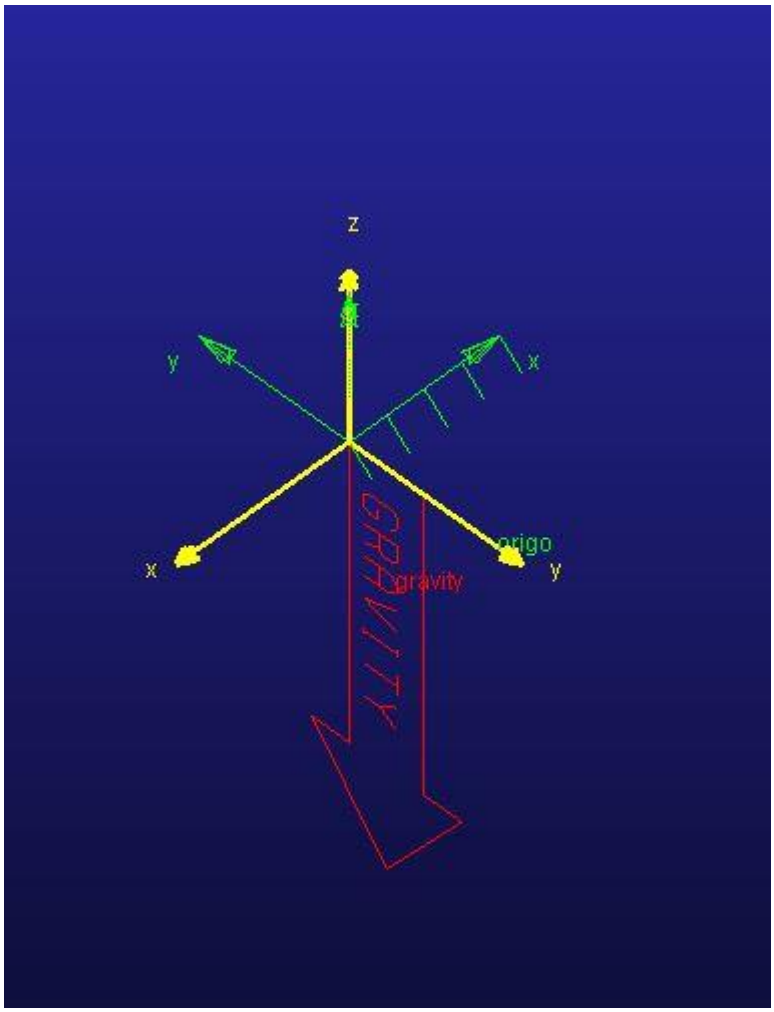

Figure 14. Adams Car origo with positive directions in yellow.

The template building was started by creating hardpoints for every part (appendices 1, 2, 3 and 4). Hardpoints are coordinate points in the space and they have only location defined with X, Y and Z coordinates. Based on the location of a hardpoint, necessary construction frames were created. Construction frames are hardpoints with orientation. Both, construction frames and hardpoints are called coordinate references. When the coordinate references were created, parts can be built based on those coordinates. They define the location and orientation for a certain part. For every part, the mass and inertia properties are defined. When a certain part, for example the lower a-arm is created, a geometry for the part can be built. With the geometry, the part is visualized in the space and its topology and movements in simulations can be

observed. If the part is connected to a body in assembly, it needs to be defined as a mount part. Mount parts are massless.

Movement between two parts (I and J part) is enabled with joints or bushings. Joints and bushings are attachments that define the number of DOFs between the I and J part. Different joints enable different DOFs in defined location and orientation. Bushings are operated with property file. Certain forces, which allow certain displacements in 6-DOF, are defined in the property file. In simulations an assembly can be set to kinematic or compliant mode. Kinematic mode uses only joints and compliant mode uses bushings and necessary joints defined under compliant group.

Force elements, such as dampers, springs and bumpstops, are also created in the template builder. Properties to them are defined with a property file. The property file contains necessary information for the functioning of the force elements. Damper property file, for example, contains force in function of velocity in designated amount of datapoints and can be seen from the figure 15. Values to those variables were calculated with Excel calculator, separately for every spring and damper.

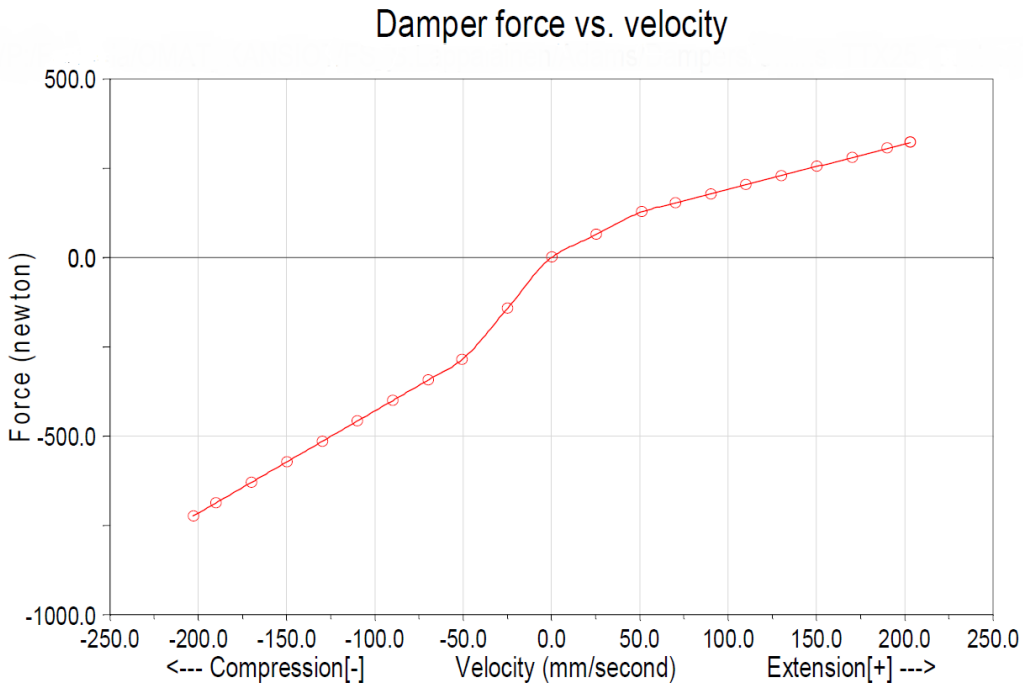

Figure 15. Front heave damper force vs velocity curve.

Other features created in the template builder were parameter variables which define desired values to certain functions, adjustable forces to define desired camber and toe angles, and output requests for observing desired features in different DOF's with a function expression.

When a model is set to a test rig or connected to other template in assembly, Adams Car operates with input and output communicators. The communicators need to be defined between the attached parts in different templates and between the test rigs, where the simulations are executed. Input and output communicators are set to connect with matching names. The front suspension template of HPF023 can be seen from the following figure 16.

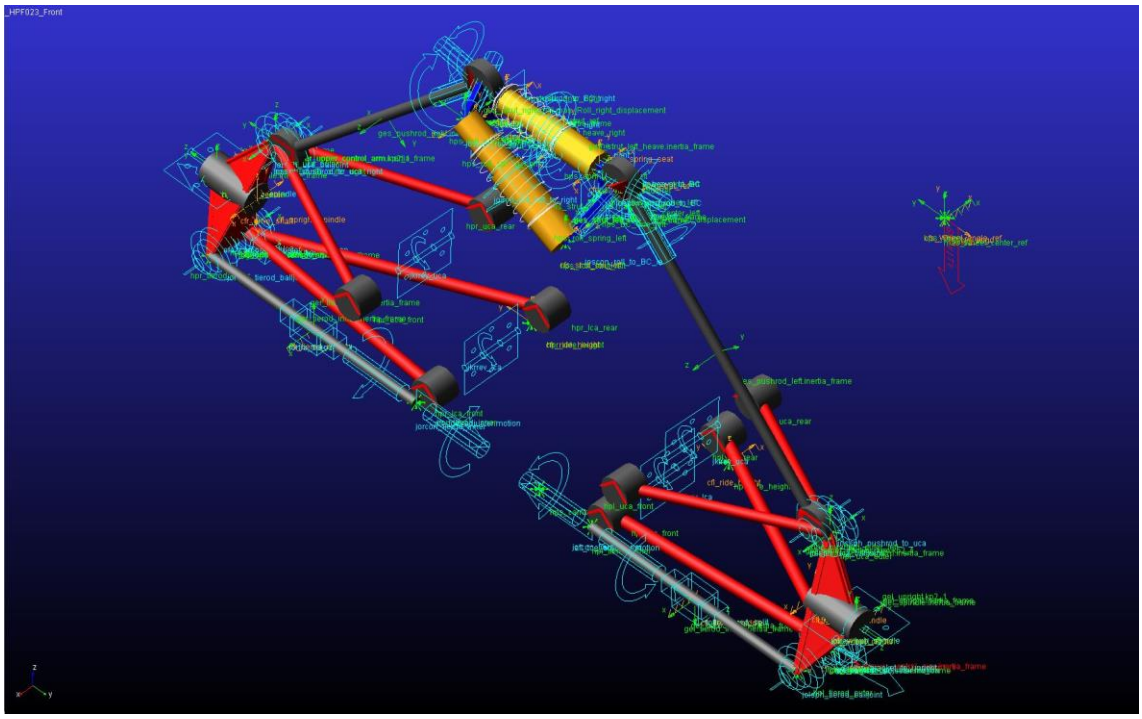

Figure 16. Front suspension template of HPF023 with toggle icons visible.

3.2 Subsystem

Another mode in Adams Car is called the standard interface. When a template is built and ready, a subsystem is created in the standard interface based on that template. The subsystem enables the executing of changes to the template without switching from standard interface to template builder. If the simulation results are not satisfying, a certain feature, for example hardpoint location, can be changed in subsystem in standard interface.

3.3 Assembly

Assembly is another feature in the standard interface. Assemblies are created from subsystems and all the simulations are completed with assemblies. Adams Car has different test rigs for every simulation. Depending on the assembly, Adams Car automatically sets a test rig to the location defined with communicators. Adams Car has a large number of built-in simulations for individual templates and full vehicle models. Adams Car then automatically animates the completed simulation. Results can be observed in the post-

processing window, where the requested variables can be plotted to the vertical horizontal grid. Suspension and steering -assembly of HPF023 on a test rig can be seen in following figure 17.

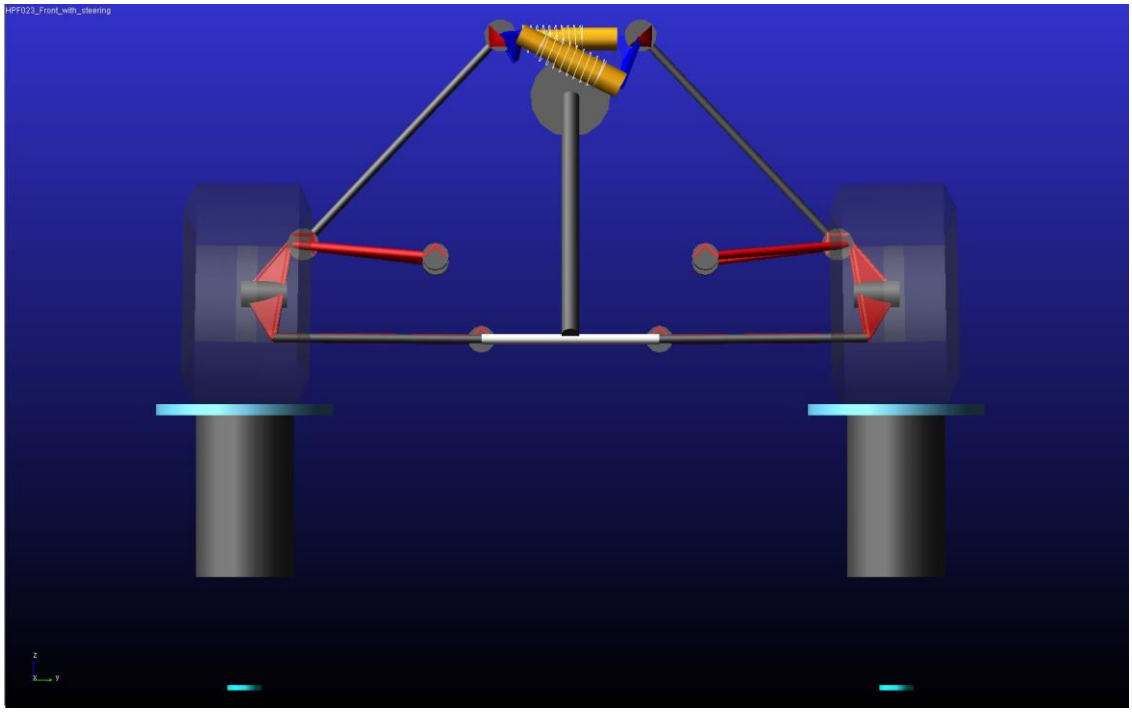

Figure 17. Front suspension with steering assembly in compliant mode.

3.4 Full Vehicle Model

Full vehicle model is a multibody model from the whole vehicle. For the full vehicle model of HPF023, templates were built for the front and rear suspension, steering and chassis. Subsystems were created from the templates mentioned above and from front and rear tire models (appendix 5). Adams Car has built-in tire models to front and rear. These models automatically created a geometry for the tire based on the tire model that is used. Tire model is a property file that contains all the information needed to describe the tire features. Property file of the Hoosier LC0 tire with all the necessary data was received from the FSAE TTC's private server (appendix 6).

Once the subsystems from the front suspension, rear suspension, steering, chassis, front tires, and rear tires were built, full vehicle assembly was created

and can be seen from the figure 18. With the full vehicle assembly, a selection of simulations can be completed. In addition, powertrain and brakes subsystems can be added to the full vehicle assembly.

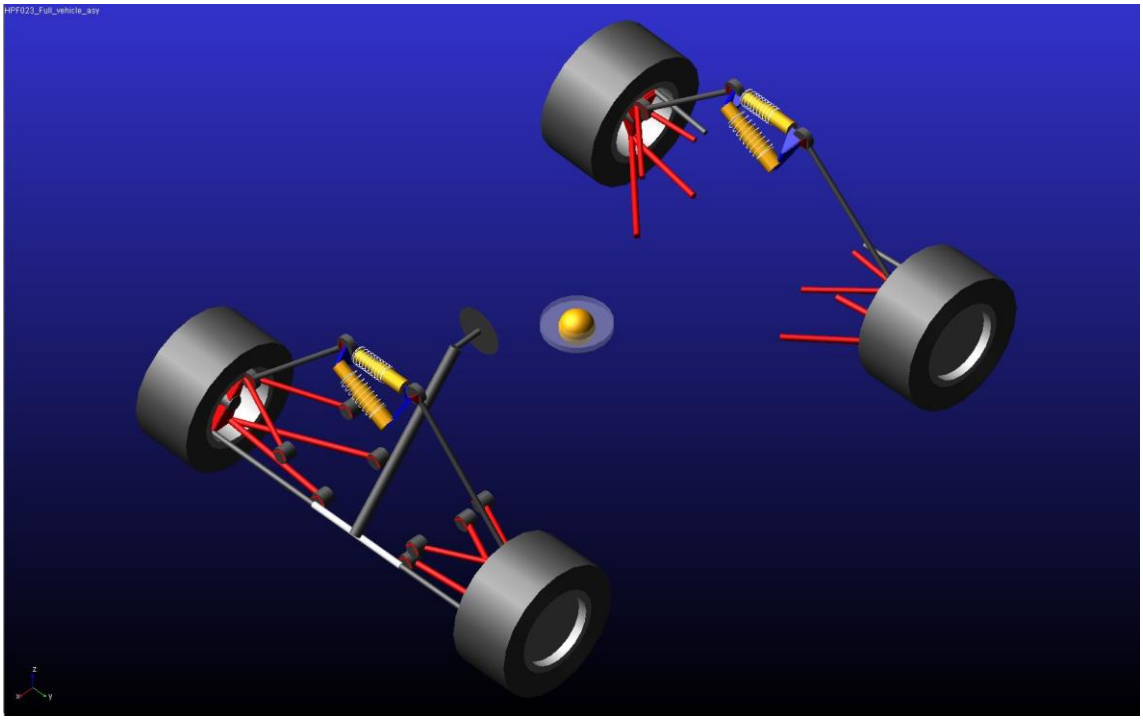

Figure 18. Full vehicle model of HPF023 with front suspension in compliant and rear suspension in kinematic mode.

3.5 Flexibility

Flexibility to the lower a-arms in front and rear suspension was created with Adams ViewFlex. ViewFlex operates with MNF-files which contain a mesh to certain part. Type, shape, order, specification, edge shape, size, growth rate and shell thickness were set to the elements used in the mesh. After the mesh properties were set, ViewFlex automatically created a mesh individually for the lower a-arms. This enabled the lower a-arms to have flexible properties. Displacement in flexible a-arm during dynamic simulation can be seen from the following figure 19.

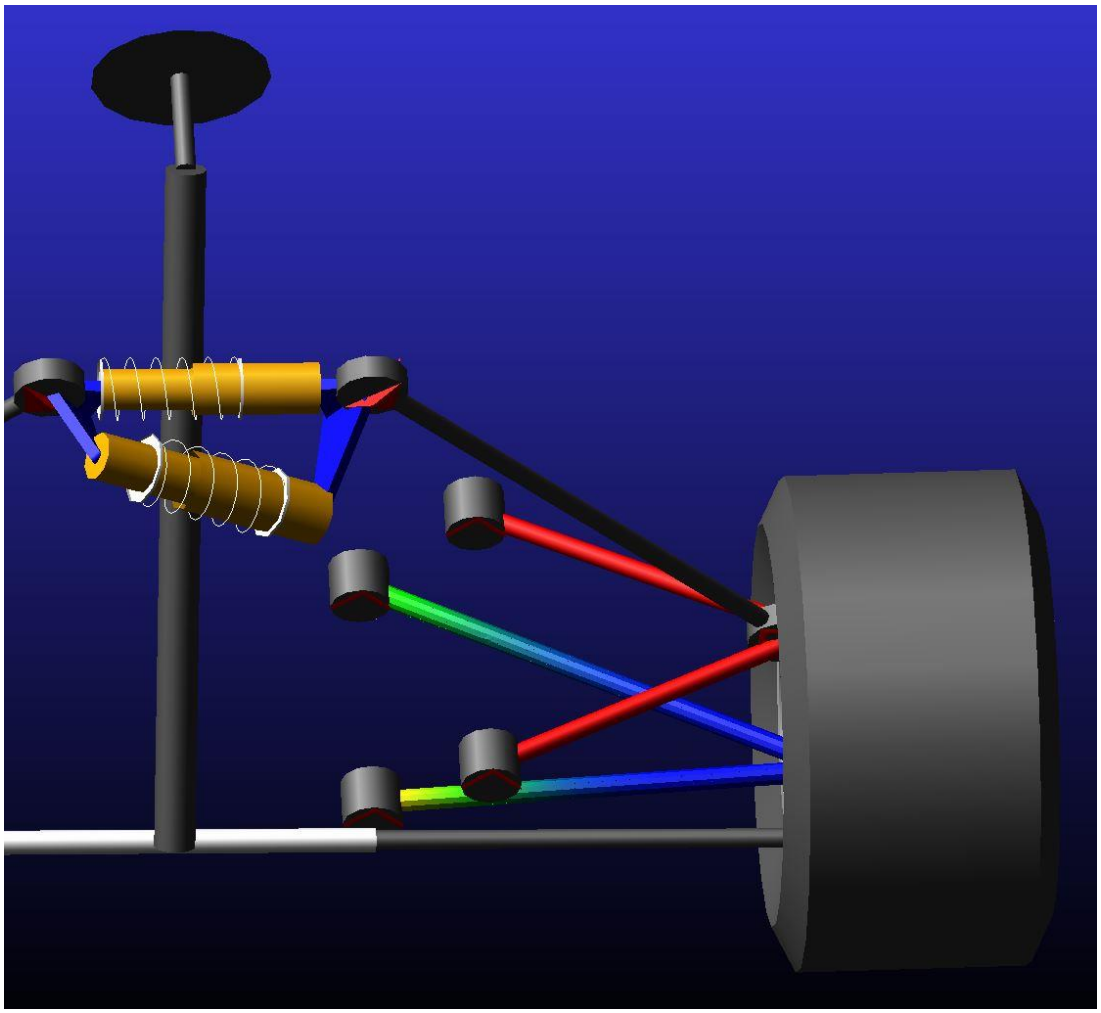

Figure 19. Front left lower a-arm's displacement during dynamic simulation.

4 Simulations

Simulations were completed in static and dynamic conditions to suspension assemblies and to full vehicle assembly. The main purpose of static simulations was to ensure that bell crank mechanisms and suspension in respect of steering and vehicle's body function correctly. The full vehicle's functioning and behaviour was examined in dynamic simulations.

4.1 Static Simulations

Initial static simulations were parallel wheel travel simulations. In parallel wheel travel simulation, the test rig raises and lowers the front or rear wheels parallelly the amount of desired bump and rebound travel. Suspension's functioning in respect to body and functioning of the heave spring-damper element were examined in this simulation. Simulations were completed on the front and rear suspensions.

In opposite wheel travel simulation, the test rig raises and lowers the left and right wheel in the front or rear axle oppositely the amount of desired bump and rebound travel. Suspension's functioning in respect to body and functioning of the roll spring-damper element were examined in this simulation. Simulations were completed on front and rear suspensions.

When the functioning of front and rear suspensions in parallel and opposite wheel travel were ensured functional, steering simulations to front suspension with steering assembly were completed. In steering simulations, upper and lower value to steering wheel's steering angle were set. The main purpose of these simulations was to ensure the steering ratio between the steering wheel and vehicle's wheels on front axle. The front suspension's functioning in respect to the body during steering inputs was also examined.

After all the necessary simulations mentioned above were completed, static load and static vehicle characteristics simulations were completed to front suspension

with steering and rear suspension assemblies. In static load simulations, Adams Car creates a load case and applies it on an assembly. A variation of forces and torques can be applied to the load case and their impact can be observed in post-processing. Braking and cornering forces to the front and rear suspension assemblies were set when the behaviour of flexible and rigid suspension arms was examined. In static vehicle characteristics rolling radius of the wheels was set and axles were being strained with a vertical force. Impact of vehicle's axle masses and weight distribution can be observed through this simulation.

For full vehicle assembly static equilibrium and static vehicle characteristics were completed before simulating the assembly in dynamic conditions. In static equilibrium vertical force caused by mass of the vehicle is straining the vehicle. Adams Car creates an analysis point so that the vehicle's characteristics caused by static vertical force can be examined. For example, the preload of heave springs and vehicle's ride height can be adjusted through this simulation. In static vehicle characteristics for the full vehicle, sprung mass to front and rear axles needs to be set in percentages. With these simulations, the impact of mass distribution can be examined.

4.2 Dynamic Simulations

Dynamic simulations were completed to the full vehicle assembly with rigid and flexible suspension arms. There are several dynamic simulation options for a full vehicle in Adams Car. The best option for a dynamic simulation is to choose a simulation that can be performed with an actual vehicle. Results from driving data and from simulations are then comparable and the simulation model can be modified until the results are satisfying and will most likely match with the data gained from the real track.

ISO lane change from course events was used to simulate the vehicle's performance. Standardized lane change was also built on the test track and driven through in several runs with HPF023. Therefore, the results from the simulations were comparable to the actual driving data. In the ISO lane change

vehicle is driven through a lane width of three meters, then changing lane to the other side of the track. The second lane's width is the width of the vehicle plus one meter (1 m). After driving through the second lane, the vehicle changes back to the original side of the track and drives through a third lane width of the vehicle's width multiplied with 1.1 and added 0.25 m to the product. All horizontal and vertical distances between the three lanes can be seen from the figure 20. The whole lane change maneuver should be completed with constant velocity. Velocity on which the vehicle is completing the lane change and step size to a simulation animation are the only parameters set to complete the ISO lane change maneuver in Adams Car.

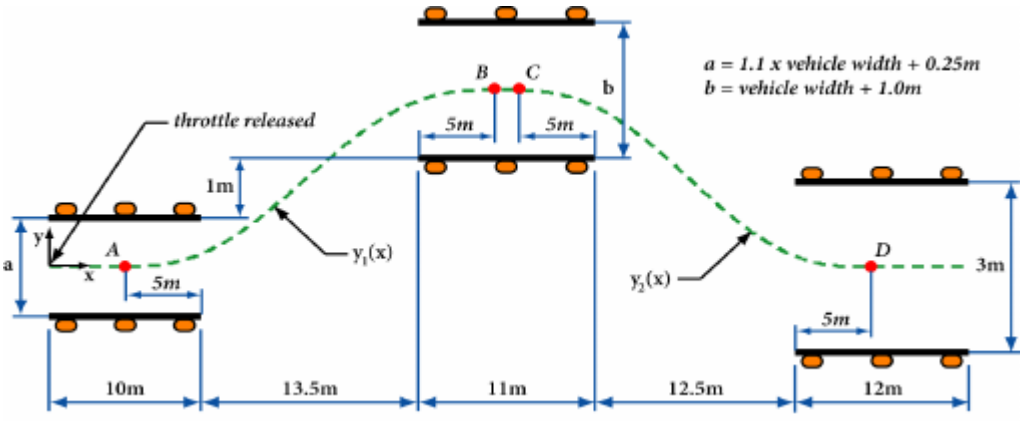

Figure 20. ISO lane change maneuver [11].

The vehicle's performance in corners was simulated with open-loop impulse steer simulations. The purpose of these simulations was to mirror corners from the real track. In impulse steer, the following parameters are set to complete the maneuver: initial velocity which is the vehicle's velocity to complete the maneuver, maximum steer value which is the peak steering input from the steering wheel, cycle length which defines the time how long the steering input is being applied, and start time which defines the time step when the steering input is being applied.

5 Simulation Results

Lower suspension a-arms were set rigid and flexible in four different simulations. Steel and carbon fibre were used as flexible material. The difference and effect to the results between the chosen materials were negligible. The main target was to examine and compare how flexible and rigid suspension arms behave in simulations and how the behaviour is impacting the vehicle's behaviour and thereby the segments of vehicle dynamics. The ISO lane change and Impulse steer simulations were completed in compliant mode to achieve results as accurate as possible compared to the driving data from the track. Cornering and braking force simulations were completed in kinematic mode to observe accurately the impact of flexibility.

5.1 ISO Lane Change

ISO lane change maneuver was completed with a constant velocity of 50 km/h on track with HPF023 and in simulations. The maneuver was chosen because it was easily implemented to the actual track and the results were comparable between the driving data and simulations. With these simulations, the veracity of the full vehicle model was observed and modified if necessary. Primary observation was made to the lateral acceleration of the vehicle which can be seen in the following figure 21.

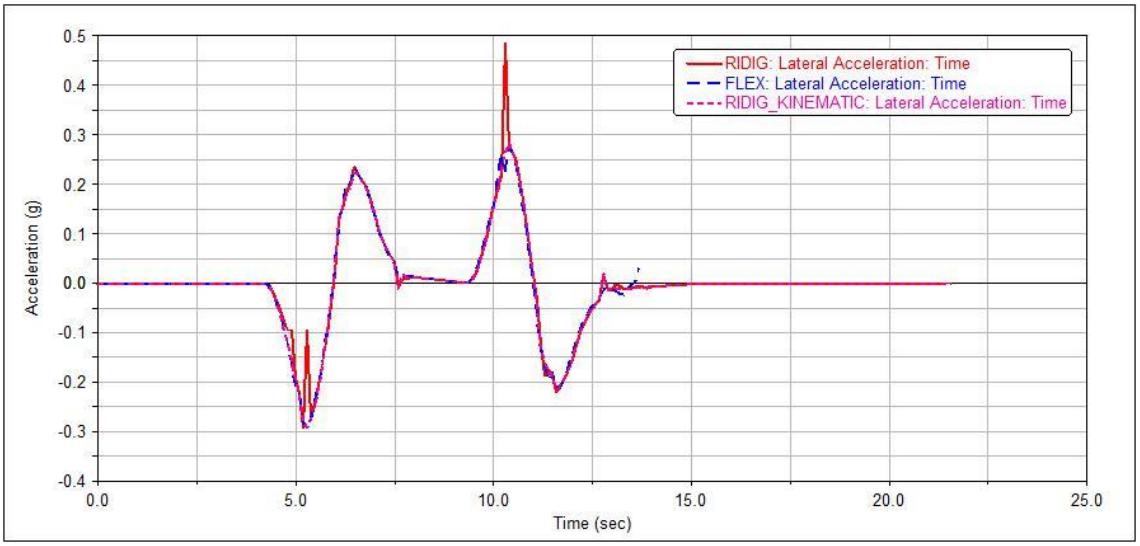

Figure 21. Lateral acceleration with different modes.

From figure 21 it can be seen that the curve of rigid arms peaks up to 0.5 g when steering input is given to the third and final lane change. Variation in values can also be seen when first steering input is given to the vehicle. It seems that the curve of rigid arms follows the values of flexible arms' curve but has sharp peaks and minor alterations during the maneuver. This can be explained with the bushings used in compliant mode. The property file of the bushings allows a certain movement when the bushing is strained with a certain force. When the arms are rigid, all flex caused by forces is directed to the bushings which causes sharp peaks during steering inputs. Therefore, additional simulation, where the front and rear suspensions were set to kinematic mode, was completed. In kinematic mode, the bushings are replaced with joints that allow zero flex. The pink curve presents the kinematic mode with rigid arms. Now it can be seen that the pink and blue curve are fairly similar and the flexibility of suspension arms does not cause any major difference to the vehicle under lateral acceleration.

In figure 22, normal force of the front left tire is being observed in a function of steering wheel angle.

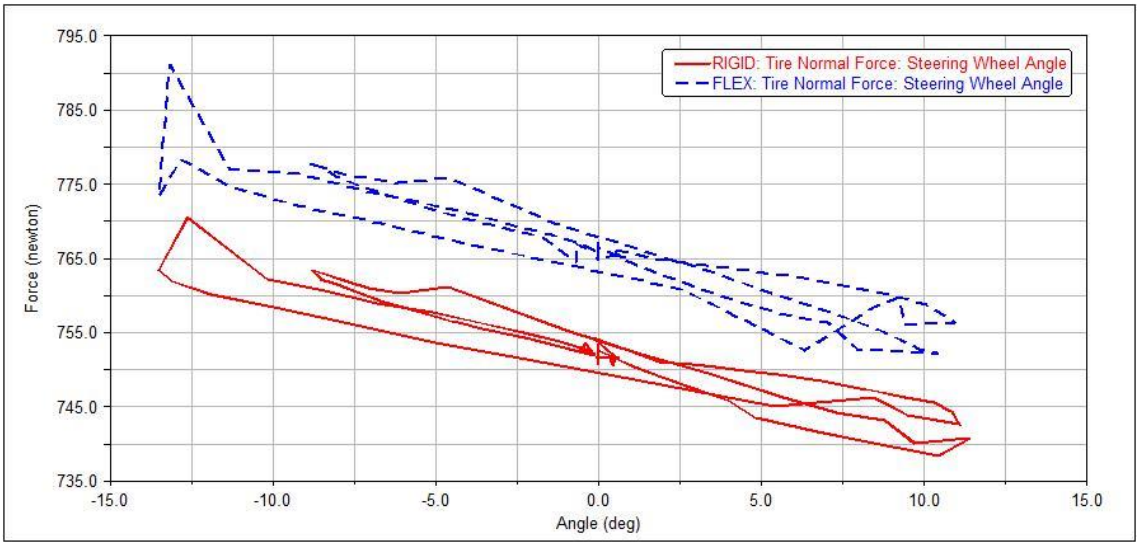

Figure 22. Normal force of left tire when steering inputs are applied.

From figure 22, it can be seen that to the left tire (which was chosen arbitrarily) of the suspension with flexible arms affects greater normal force, which means it also needs to produce more tire forces than the suspension with rigid arms. The difference can be explained with dynamic wheel load transfer. Certain amount of tire forces exists and depends on the force caused by acceleration which is explained in chapter 2.2.2. Therefore, the magnitude of forces caused by the wheel load transfer is the same but occurs on different wheel. With softer arms, in this case flexible, less force distribution occurs between left and right tires. Flexible arms maintain greater tire force during the maneuver because the movement of the vehicle's body is softer.

5.2 Impulse Steer

One specific corner from the test track was simulated with impulse steer, so that the simulation results can be compared to the driving data. In simulations, the duration of the maneuver was set to 9 seconds, velocity on which the maneuver was completed, maximum steering angle from the steering wheel and duration of steering input was taken from data and set to 45 km/h, 45 degrees and 3 seconds. The time step of when the steering input is being applied was set to 2 seconds. The tire's ability to produce lateral force in a function of slip angle during the

maneuver was the first condition being observed. Results can be seen in the following figure 23.

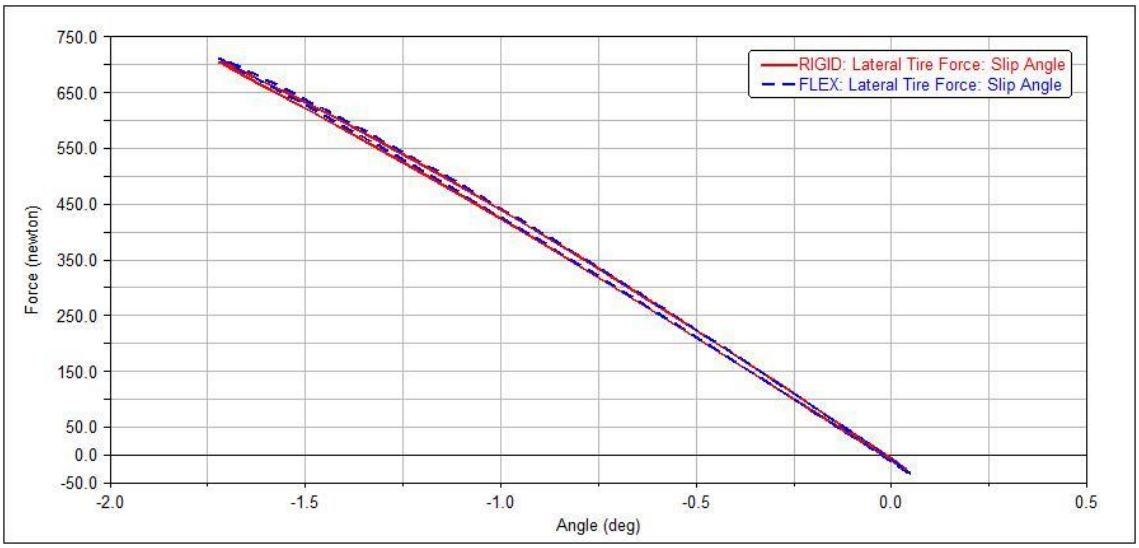

Figure 23. Lateral force production in different slip angles.

From figure 23 it can be seen that the flexibility of the lower suspension arms does not cause major difference to the tire's ability to produce lateral force during different slip angles.

The lower a-arm's front bushing's displacement in Y and Z directions in a function of lateral tire force can be seen from the following figure 24.

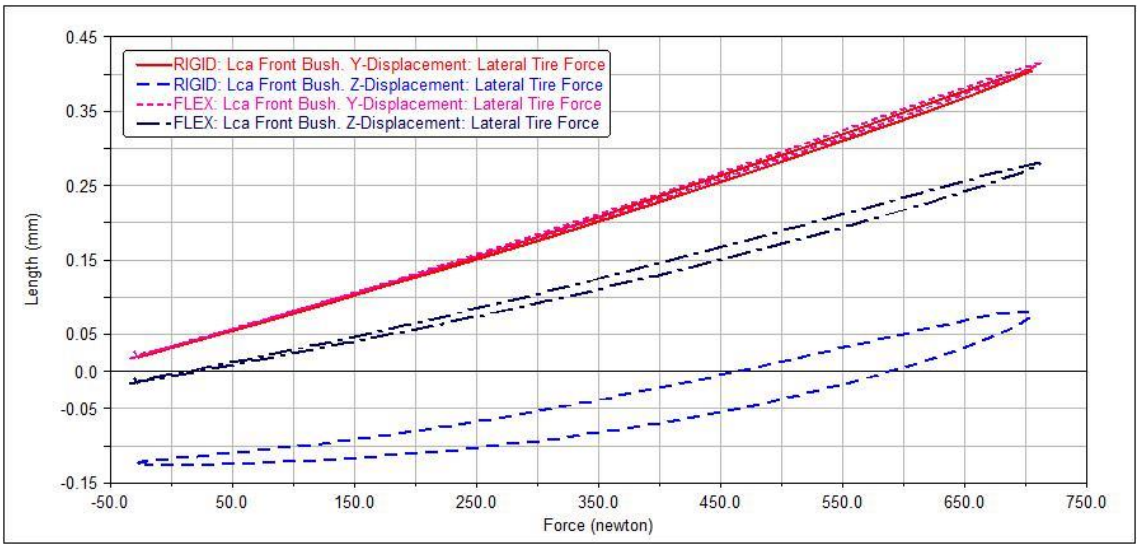

Figure 24. Lower a-arm's front bushing's X and Y displacements.

From figure 24 it can be seen that the difference in a-arm's front bushing's displacement in Y-direction between rigid and flexible is not major. Larger differences can be seen in Z direction's displacement. Similar results were received from the rear axle of the vehicle which can be seen from the following figure 25.

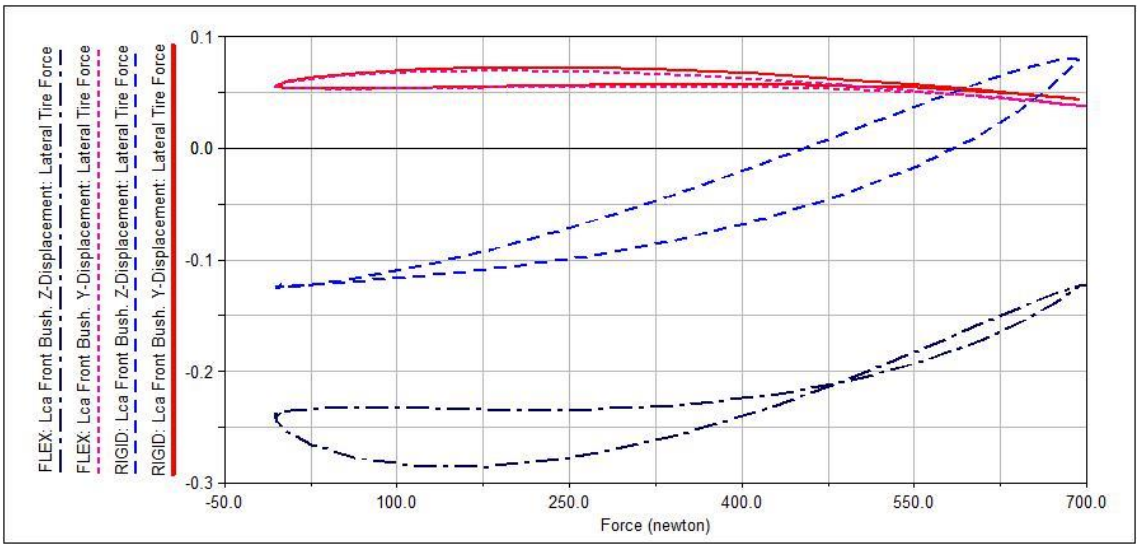

Figure 25. Lower a-arm's front bushing's X and Y displacements on the rear axle.

The figure above shows that the difference in Y displacement between rigid and flexible arms stays more or less the same as on the front axle. In Z displacement a difference compared to the front the axle can be noticed. Static load causes minor Z displacement to the flexible arm because its initial displacement when almost non force is applied differs from zero. In this simulation, the displacements caused by bushings need to be taken into account. The displacement of rigid arms occurs only because of the bushings between the arm and vehicle's body. The simulation could have been completed in kinematic mode where joints replace bushings. The displacement of rigid arms would be closer to zero in that case.

Then impact of flexible lower a-arms to rigid upper a-arms was examined in the following figure 26.

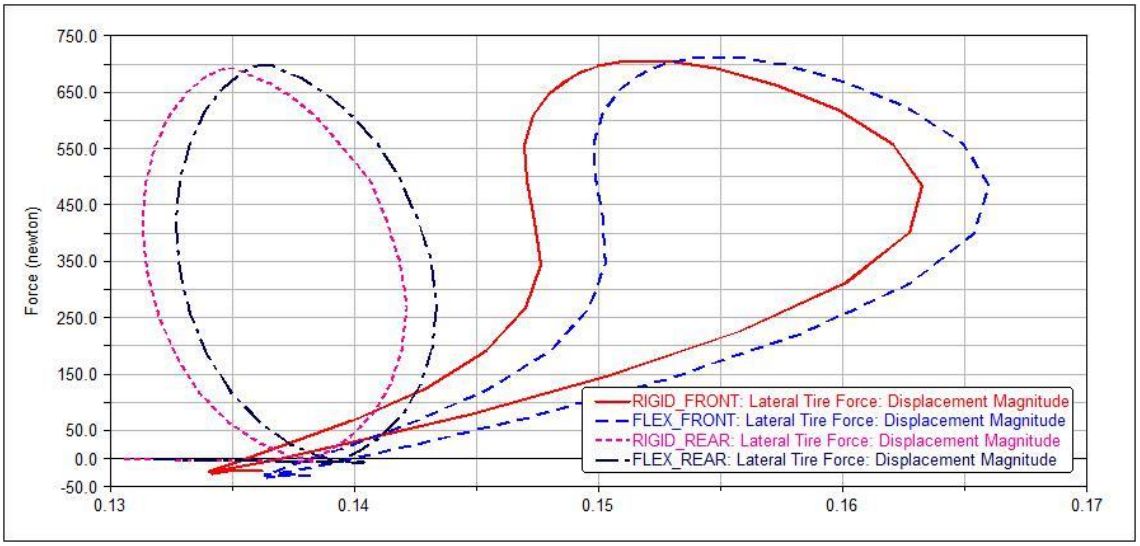

Figure 26. Displacement of upper a-arm.

In figure 26, lateral tire force in a function of displacement magnitude of upper a-arm is being examined. Figure 26 shows that the flexibility of lower a-arms is not causing deviant displacements to other suspension arms.

The yaw Rate change during the simulation can be seen from the following figure 27.

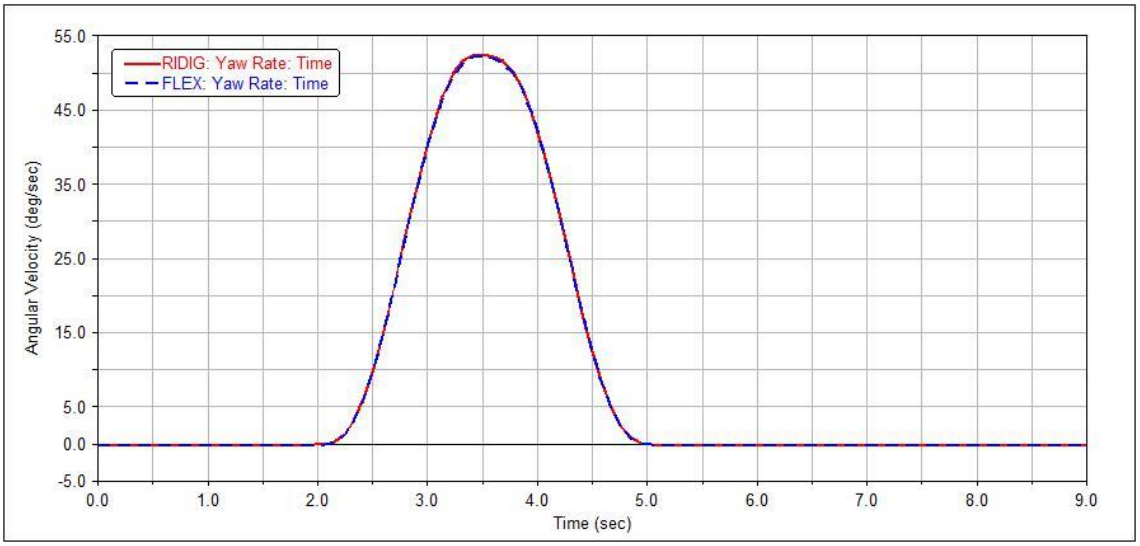

Figure 27. Yaw rate with rigid and flexible lower a-arms.

Figure 27 shows that the yaw rate of the vehicle does not vary between the rigid and flexible lower a-arms. This can be assessed as a desired result. Major forces,

displacements and differences between flexible and rigid arms will occur in conditions where the vehicle receives its maximum values in longitudinal and lateral accelerations. These aspects are examined in the following chapters.

5.3 Cornering Force

Cornering force simulations were based on the vehicle's lateral acceleration and the maximum lateral acceleration values were gathered from driving data. The maximum and minimum forces caused by acceleration of 5950 N and -5950 N were the only parameters set and impacted the left and right side of the axles. In the following figure 28 the lateral displacements of the left wheel center in a function of lateral force can be seen.

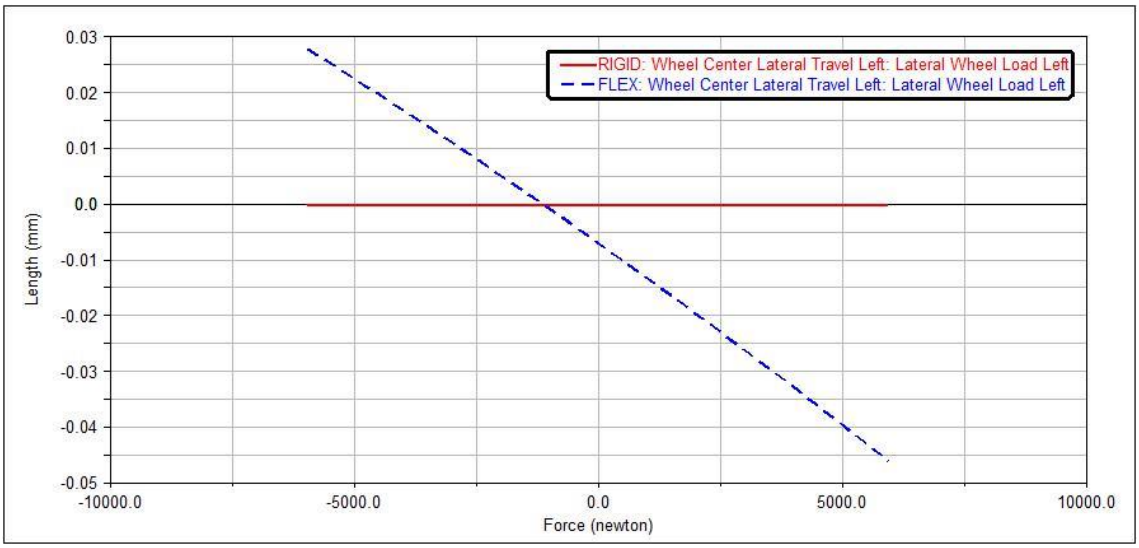

Figure 28. Lateral displacement of left wheel center caused by lateral wheel load.

In kinematic rigid suspension, zero displacement occurs during cornering. In the flexible arms, displacement can be observed instead but the magnitude of it is insignificant. Minor displacement can still cause transition in other aspects related to vehicle's ability to perform and maximize grip. The impact of flexibility to the wheel's camber angle can be seen from the following figure 29.

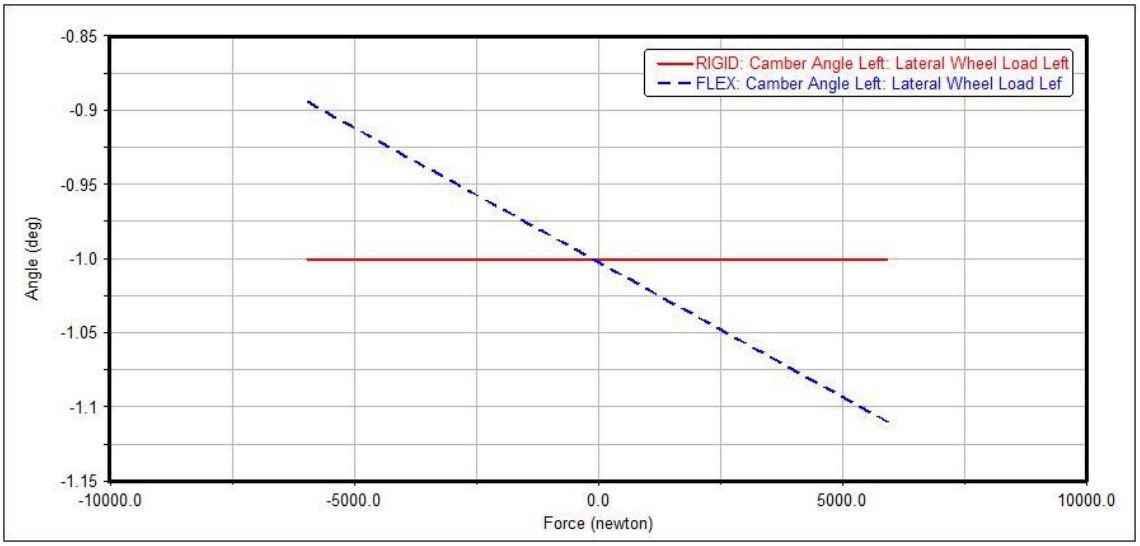

Figure 29. Camber angle change caused by lateral wheel load.

Variation of 0.2 degrees in camber angle can be seen when lateral acceleration achieves its positive and negative peak values. The camber gain of the wheel can be seen in a more demonstrated way in the following figure 30.

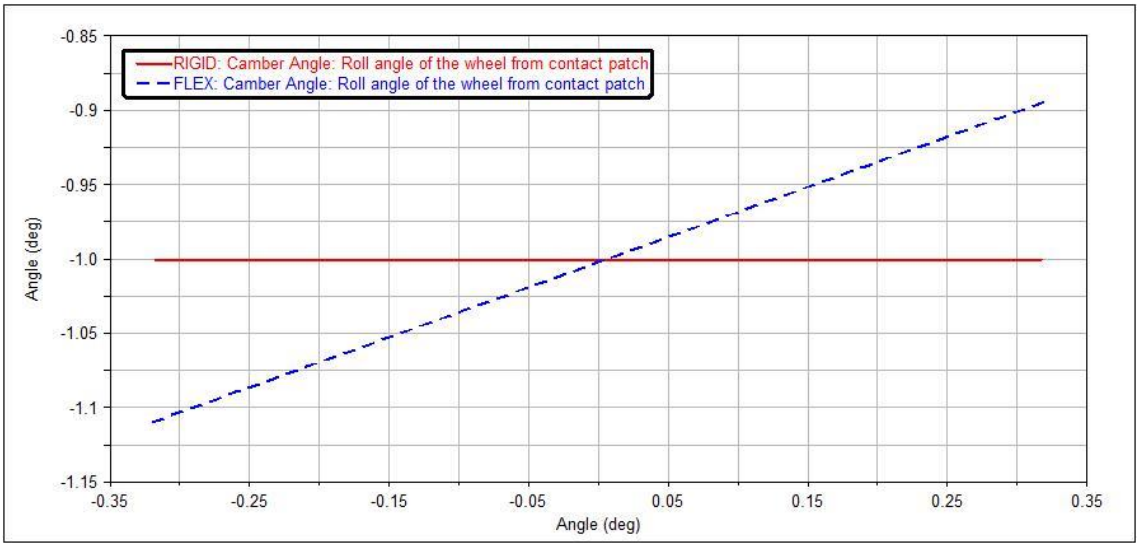

Figure 30. Camber gain of the wheel.

Figure 30 shows that flexible arms enable camber gain of the wheel in terms of roll spring rate when the wheel acquires vertical displacement. The change in camber angle follows the vehicle's roll displacement approximately 0.1 to 0.2 degrees behind. Simulation in compliant mode would have increased the camber gain of the wheel but the purpose of this simulation was to illustrate the impact of

flexibility. In motorsport, it is desirable to achieve matching camber gain compared to vertical displacement of a wheel. Therefore, the wheel has its entire contact patch in contact with road.

Alongside with camber, toe angle is a basic adjustment in suspension especially in racing vehicles. The impact of flexible arms to toe angle change can be seen in figure 31.

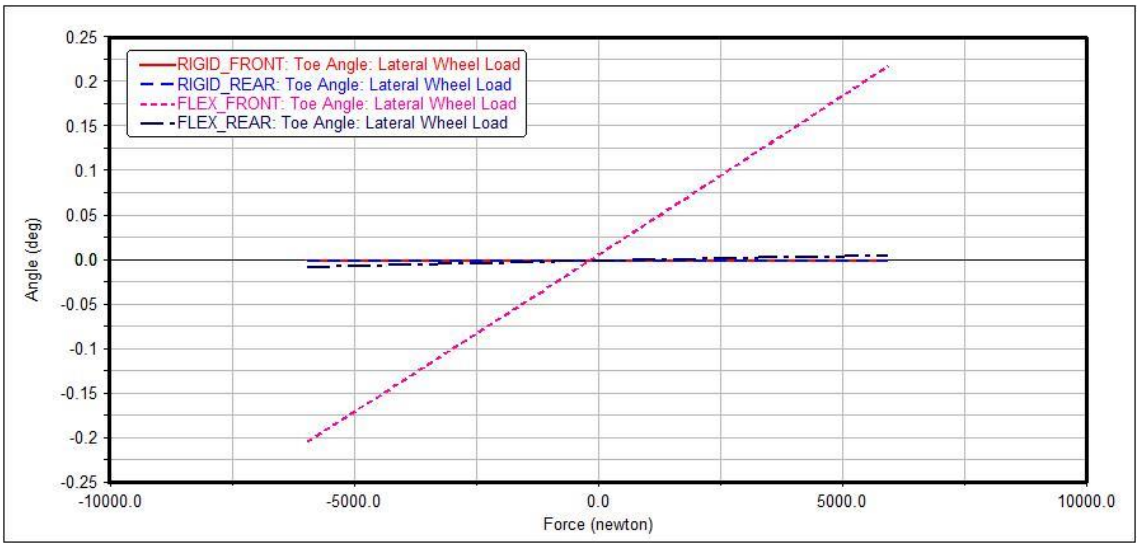

Figure 31. Change of toe angle.

Flexibility of suspension arms causes a minor change in the vehicle's toe angle on the front axle and negligible change on the rear axle.

Change in Ackermann in a function of lateral wheel load can be seen in the following figure 32.

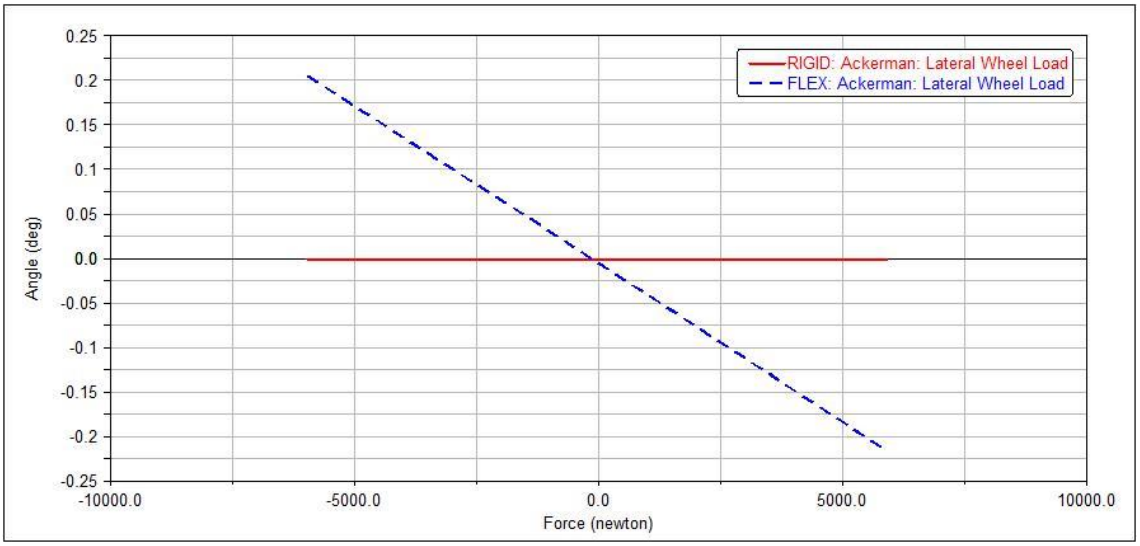

Figure 32. Change of Ackermann.

As the figure above shows, lateral acceleration causes minor deflect to Ackermann geometry with flexible a-arms. HPF023 has certainly minor Ackermann steering geometry, and as it can be seen from the results with rigid arms steering, the geometry is more or less parallel.

The total suspension roll rate in a function of lateral wheel load can be seen in figure 33.

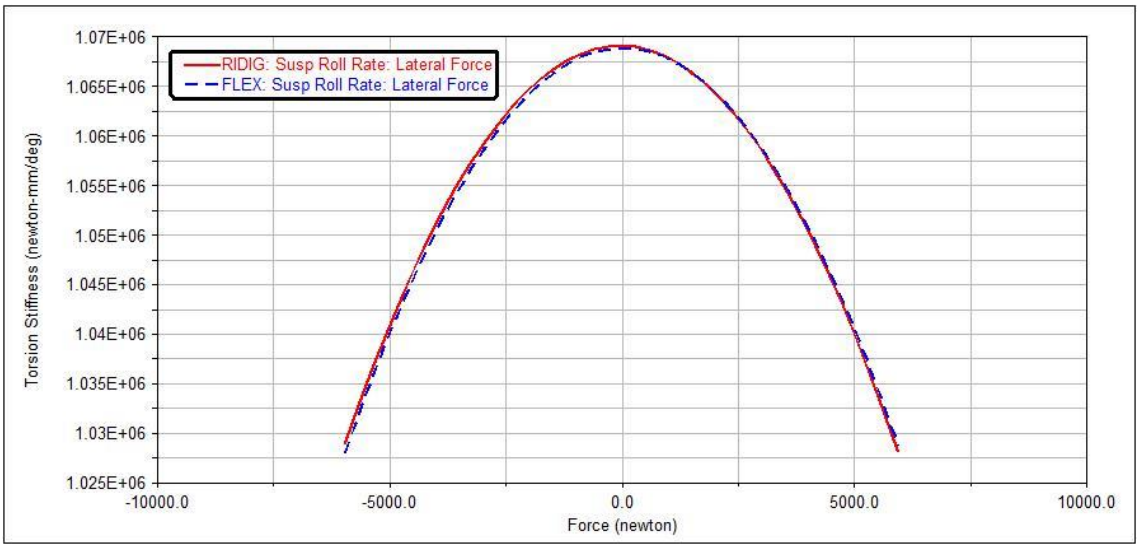

Figure 33. Change in total suspension roll rate.

Figure 33 shows that the flexibility of the lower a-arms does not cause major impact to the total suspension roll rate meaning the combined roll rate of the front and rear suspensions.

5.4 Braking Force

Braking force simulations were based on the vehicle's longitudinal acceleration and maximum longitudinal acceleration values were gathered from driving data. Maximum and minimum values to reaction force were set to 5000 N and -5000 N. The positive value is for acceleration and the negative value the deacceleration (braking). These were the only parameters set to the simulation. Wheel center displacement in a function of longitudinal wheel load can be seen from the following figure 34.

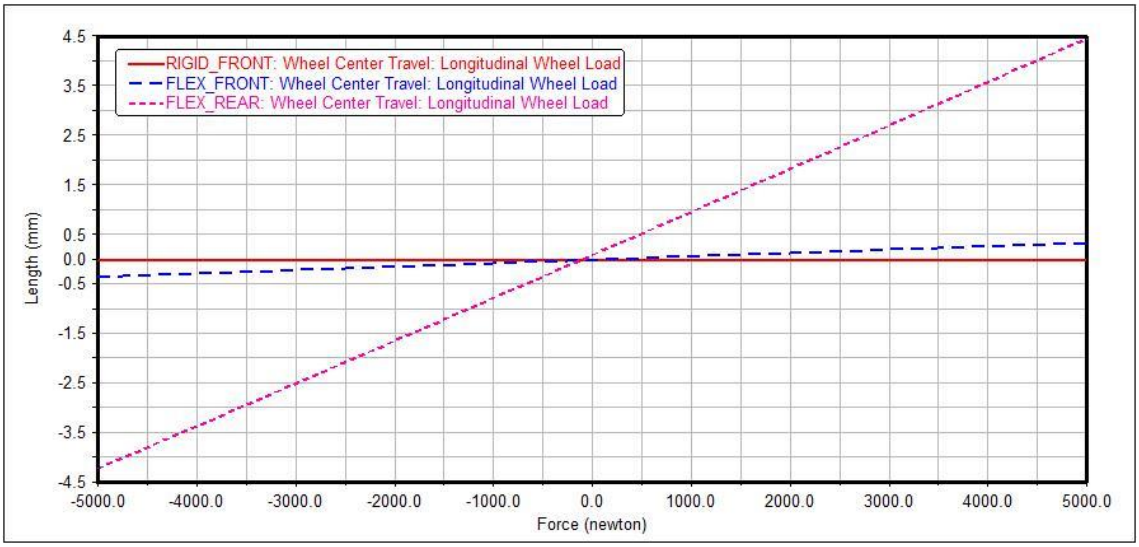

Figure 34. Longitudinal displacement of wheel center.

Figure 34 shows that minor displacement on the front axle can be noticed. Rear axle, instead, suffers surprisingly major displacement. The driving ratio and braking balance was set to 50 % per each axle. This may explain the displacement in the rear suspensions' a-arms.

The caster angle in a function of longitudinal wheel load can be seen from the following figure 35.

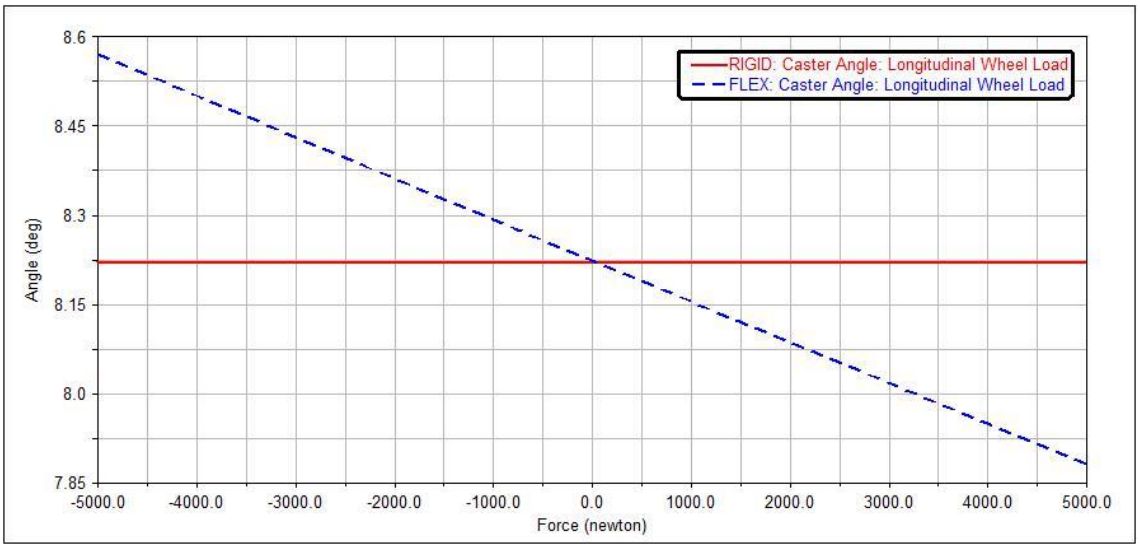

Figure 35. Change of caster angle.

From figure 35, it can be seen that the acceleration and deacceleration (braking) of the vehicle are causing approximately 0.35 degrees of change to the caster angle. This affects the self-aligning torque which increases or decreases the stability of the vehicle depending on the acceleration. King pin inclination, which is similar to caster angle but from the front view, can be seen from figure 36.

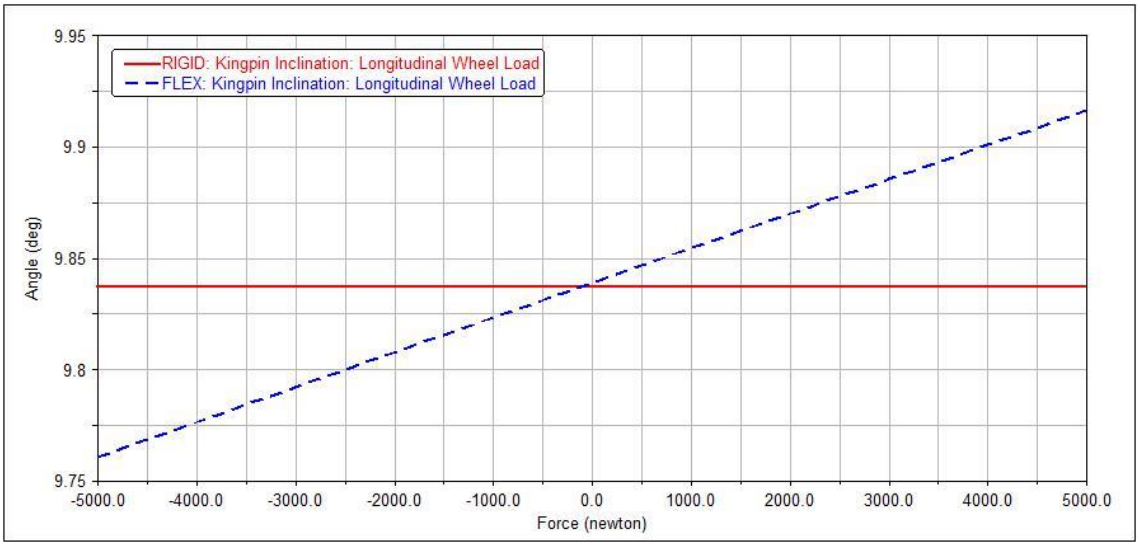

Figure 36. Change of king pin inclination.

Impact to kingpin inclination change is opposite to caster angle change. Under braking, the kingpin inclination is decreasing and in acceleration increasing. Both

of these aspects cause the rise and fall of the wheel. Another aspect related to the king pin inclination is scrub radius which can be seen from the following figure 37.

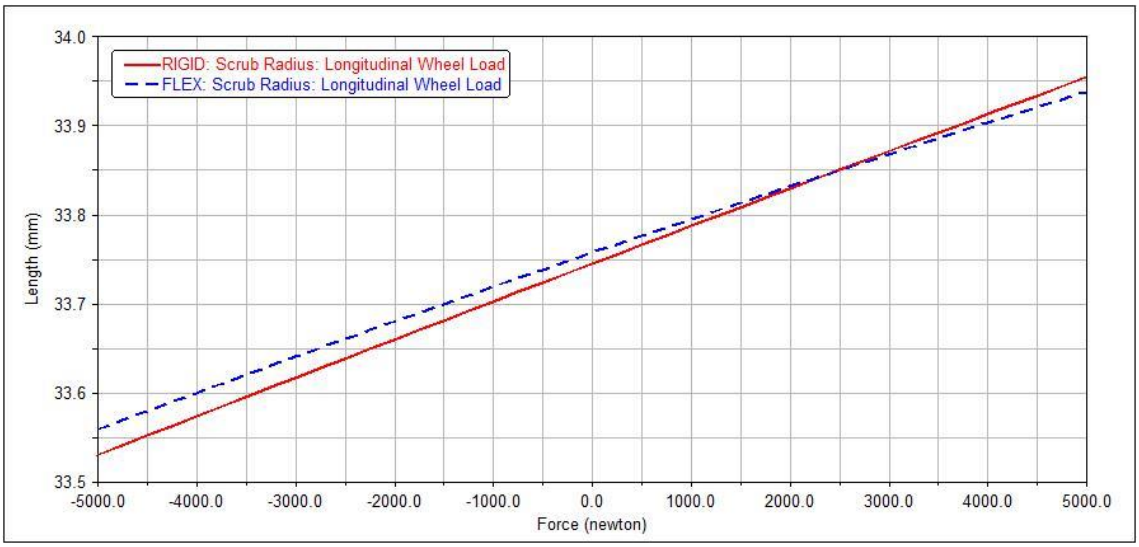

Figure 37. Change of scrub radius.

Figure 37 shows the change of scrub radius in a function of longitudinal wheel load. The difference between rigid and flexible arms is negligible and hence flexibility of a-arms is not causing any addition to the vehicle's behaviour under braking conditions.

Anti-geometries in a function of longitudinal wheel load can be seen in the following figure 38.

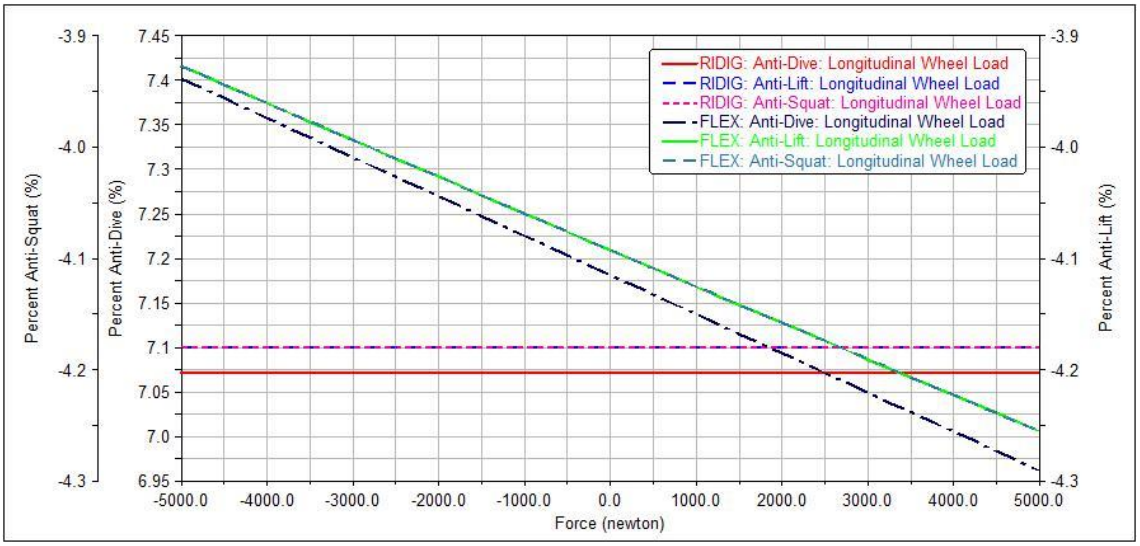

Figure 38. Change of anti-geometries.

Anti-geometries are the features affecting the vehicle when it is accelerating or braking. From figure 38, it can be seen that the impact of flexible arms is causing a change of few decimals to the anti-geometries. The magnitude of change can be considered still quite insignificant.

6 Simulations and Testing Data

6.1 Simulation Problems

Simulation models are built to match with a vehicle as accurately as possible. There are still several factors occurring which make the modelling difficult or almost impossible to match with the actual vehicle or driving conditions depending on the software that is used for the simulations. In Design Events at Formula Student competitions simulations are the basis to succeed. Using resources to create and improve simulation models is mandatory if the team is pursuing success.

All the results from simulations are indications from the parameters that are set to the simulation models. The parameters are calculated or desired values, or values gained from testing data from the track. Data from various circumstances from the track may be difficult to execute in the simulations. Several factors can cause minor errors to the values that are set to the simulations and a sum of multiple minor errors may lead to biased results. Simulation results can be then compared to the vehicle's performance on track. The vehicle is examined with multiple sensors and those needs to be plugged, tuned and calibrated correctly to gain data that is beneficial and comparable. Parameters set to the simulation, whether they are desired, calculated or gained one way or another, may contain faults caused by human errors. Validation and iteration of simulation parameters and collected driving data is compulsory and will eventually lead to highly accurate and comparable results between the simulation results and driving data. This process demands remarkable amount of time and resources but is beneficial when design decisions can be examined and explained with results gained from simulations.

6.2 Comparison to Calculations and Testing Data

Target values where to aim were based on a previous vehicle's test data, the team's previous experiences and new calculations when the design of HPF023

was made. Targets are valuable and compulsory material in design events at FS competitions. Regarding calculated values, it needs to be taken into account that in the real world there are multiple factors which affect the final results in this case to the vehicle. Some static characteristics can be compared with high accuracy between calculated values and static full vehicle simulations.

The total roll rate of suspension was desired to be around five times softer compared to the monocoque's roll stiffness based on different sources and the team's previous experience related to the design of FS vehicles. Initially, the monocoque's roll stiffness of 5370 Nm/deg was received from a simulation made with Siemens NX. The front and rear suspension roll rate was desired to be the same, thereby the initial value to front and rear roll rate was 537 Nm/deg. The roll rate of 541.4 Nm/deg to front suspension and roll rate of 566.2 Nm/deg to rear suspension was received from Adams Car full vehicle static simulation. Roll gradient and roll springs stiffness calculations were based on those roll rate values.

Pure lateral force production of the tire can be observed with the tire testing results received from FSAE TTC private server. The following figure 39 shows Hoosier LC0's lateral force production in a function of slip angle in laboratory circumstances.

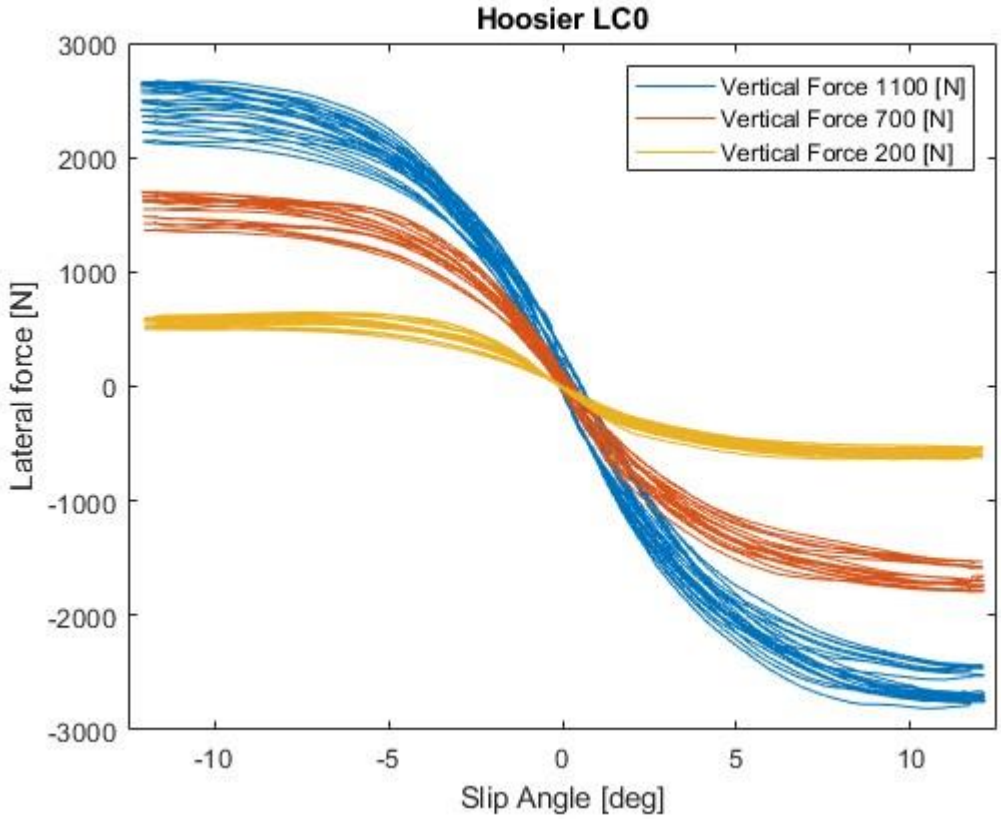

Figure 39. Lateral force production of Hoosier LC0 tire.

Curves in figure 39 are with minimum 200 N and maximum 1100 N of vertical forces and also with vertical force of 700 N which corresponds approximately the vertical force of HPF023 for one wheel in static conditions. Variation in the results with the same vertical force is caused by several test sweeps. During the sweeps, the tire warms up and is capable of producing more lateral force. More exact observation can be made with slip angles from the impulse steer which is explained in chapter 5.2 and results from the tire data can be seen in figure 40.

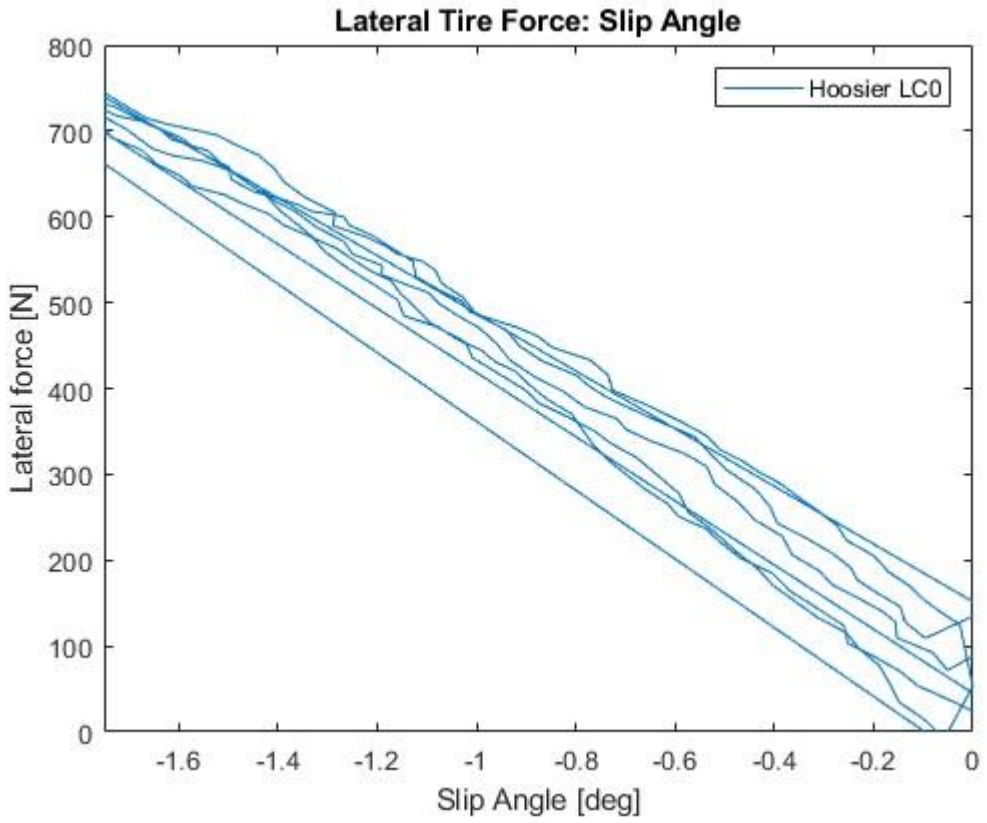

Figure 40. Lateral production of Hoosier LC0 tire with similar wheel loads from impulse steer.

As figure 40 shows, the lateral force production of the tire reaches more or less similar peak values with similar slip angles as in impulse steer simulation. The vertical forces used in figure 40 were not perfectly matching with forces in the simulation because the tire testing was executed with certain wheel loads between approximately 200 N and 1100 N. Pure force production of the tire was assumed slightly higher compared to the simulation results from Adams and to HPF023. The tire testing is executed in pure laboratory circumstances where, for example, the differences in the surface remain the same during the whole test. Other aspects caused by the vehicle and its properties are not affecting the tire similarly in tire testing even though the tire is stressed with several vertical forces.

Hoosier LC0 was tested with the camber angles of 0°, 2° and 4°. The impact of camber angle to the production of lateral force can be seen from the following figure 41.

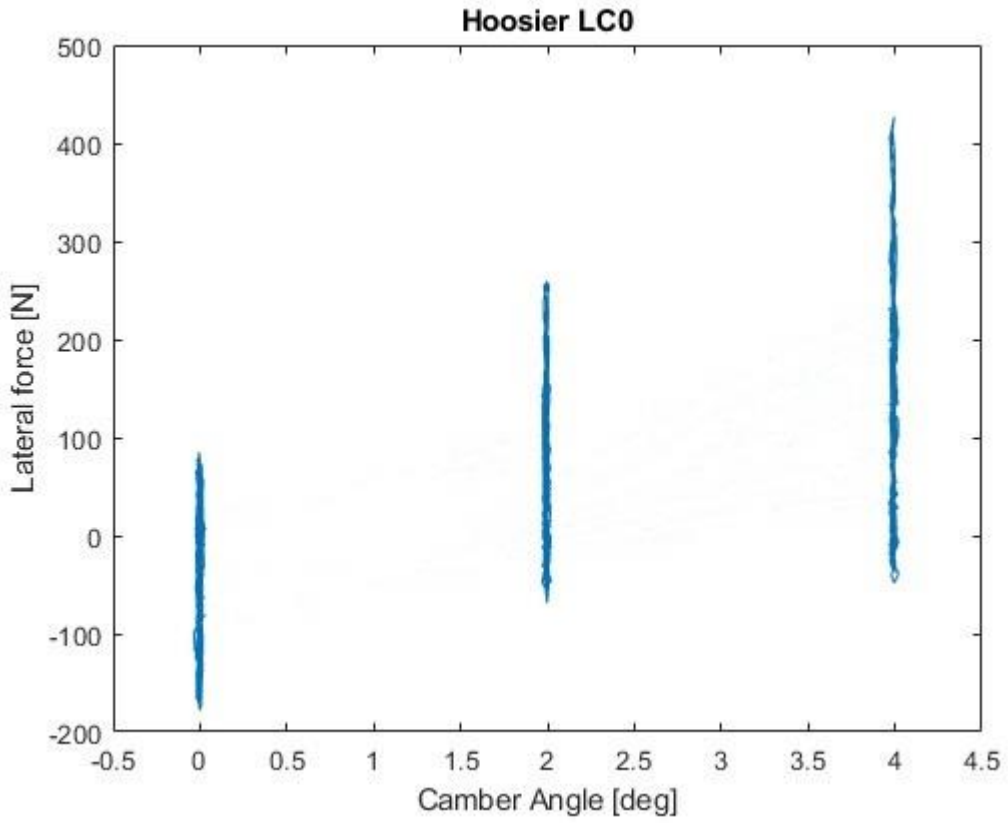

Figure 41. Camber angle's impact to lateral force.

As it can be seen from figure 41, increasing the camber angle enables the tire to produce more lateral force with certain slip angle and with varying vertical force. Due the fairly large steps between the camber angles in tire testing, its impact with more minor steps to lateral force is difficult to make proportional and hence slightly difficult to compare with results received from Adams. Flexible arms caused approximately 0.2 degrees variation to the camber angle in simulations received from Adams which can be concerned somewhat insignificant in pure tire testing.

The ISO lane change was completed on track with HPF023. Lateral acceleration values from the maneuver can be seen from the following figure 42 inside the symbolised area.

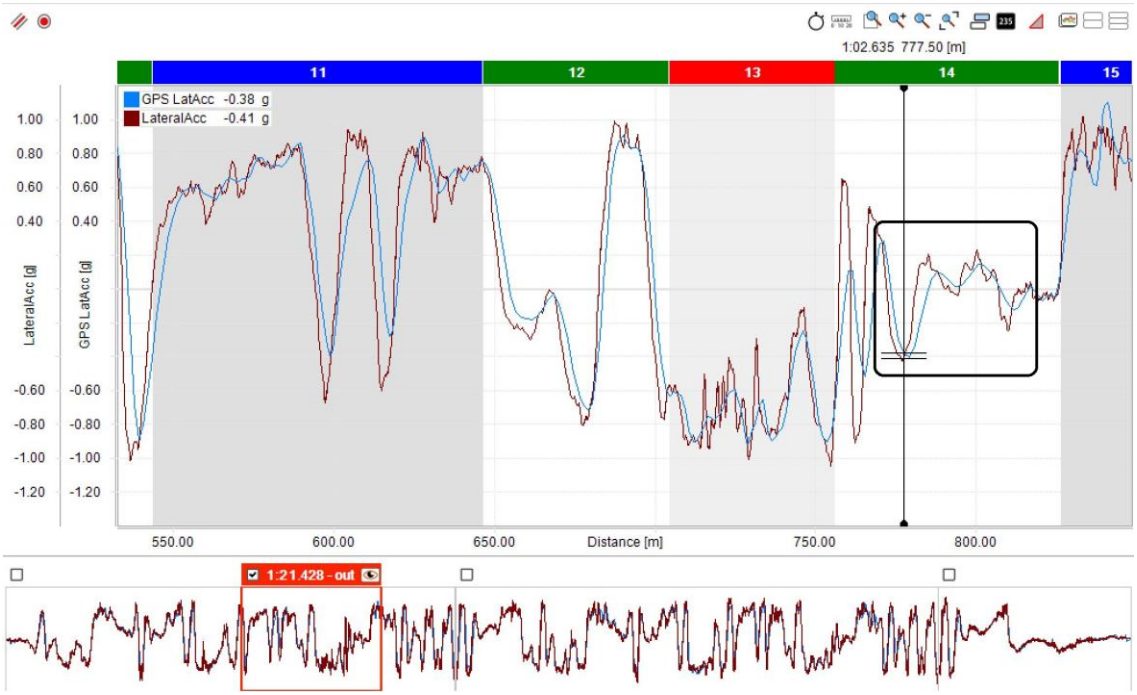

Figure 42. Lateral acceleration values from the track.

Data was collected with AIM Solo 2 data logger and inertia measurement unit (IMU) and then analysed with Race Studio 3 software. Variable “GPS LatAcc” is the data from AIM Solo 2 and “LateralAcc” is the data from IMU. Figure 39 shows that lateral acceleration values are close to the values received from the ISO lane change simulations which can be seen from chapter 5.1. Curves decreasing towards the end of the maneuver can be explained with velocity of the vehicle which is slightly decreasing. Velocity is difficult to maintain perfectly constant by a driver without cruise control. Figure 39 also shows the difference between the values collected with the data logger and IMU at the same point of the track. The data logger is located on the vehicle’s dashboard and IMU on the floor of the vehicle, as middle as possible. Different locations of measuring devices and the measuring tolerances are the main factors causing differences in the collected data.

Yaw rate from a certain corner on the track can be seen from the following figure 43 inside the symbolised area.

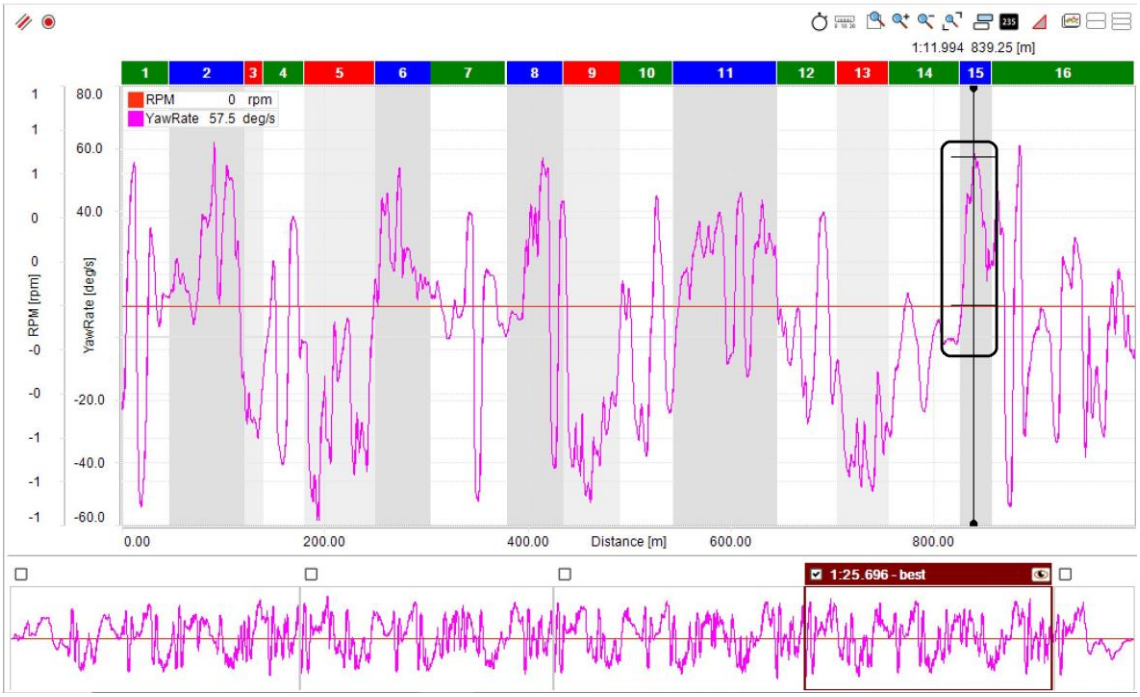

Figure 43. Yaw rate values from the track.

Impulse steer simulation was introduced in chapter 5.2 and the purpose was to simulate a certain corner from the test track which was driven through with HPF023. Yaw Rate data was collected only with IMU and its maximum value peaks at 57.5 deg/s. The peak value from the simulation was approximately 54 deg/s and the difference between values is around 3.5 deg/s. Impulse steer simulation is slightly difficult to get to match precisely with the actual corner from the track. Before and after the designated corner there are other elements that demand steering inputs, therefore a clean maneuver was not completed with the HPF023 where before and after the maneuver the track is clean and straight.

Accuracy between the simulation model of HPF023 and HPF023 would be better to clarify by running course events that model driving performance from a longer stint. This, however would go beyond the scope of this thesis.

7 Conclusions

Two main targets separated this thesis. Building a realistic and functioning full vehicle model with MSC Adams was the initial target. Creation of the simulation model was started by building templates for the front and rear suspensions, steering and vehicle's body. Suspension templates created in the decoupled suspension innovation project made by the author were used as a basis and then modified. Adams Car offered a built-in template for the vehicle's body which was then modified to match the properties of HPF023's body. The steering template was created from scratch. When the topology to every template was created and modified, the functioning of suspensions and steering was tested with suspension analysis simulations. After that, more specific parameters and property files were set to subsystems. Built-in tire model subsystems were also used with a property file that contained PAC2002 tire model from Hoosier LC0 tire.

When the suspension analysis simulations gave satisfying results and the functioning was desirable, the subsystems were combined to a full vehicle model. Simulations to confirm that all the subsystems are functioning correctly relative to each other were completed with the full vehicle model. Minor modifications were made before the dynamic simulation results were analysed. Therefore, ready-made and functioning simulation model of HPF023 devolves to the use of Metropolia Motorsport for the future revisions and development.

Comparison between the flexible and rigid suspension arms from the received simulation results was another main target. Flexibility was created with MNF-file which contains mesh and material properties. Material properties could have been measured with physical strain and compression tests but due to scheduling reasons it was settled to use values gained from different sources. Results received from the simulations regarding the impact of flexibility to displacements, forces and subjects of kinematics and vehicle dynamics seem to be reasonable.

The tire's behaviour and capability to produce forces was discovered from tire data which expresses the pure limit values of the tire. With different vertical

forces, the tire's force production was analysed and plotted with alternating slip and camber angles. The tire was able to produce lateral forces in a range from -3000 N to 3000 N with the vertical force from -200 N to -1100 N and with the slip angles from -12 deg. to 12 deg. When the capability limits of the tire were recognized, the Adams simulation results exceeding these values can be considered to result from other factors. Adams simulations with rigid arms express the results when the vehicle and its properties are in addition affecting to the force production and thereby to the kinematics. Simulations with flexible arms then express the impact of elasticity in addition to the results received with rigid arms. For comparing results to actual flexibility, several sensors would be needed to implement and install to the HPF023 when driving on the track.

References

1 Tyre slip angle. Suspension Secrets. Available from: https://suspensionsecrets.co.uk/tyre-slip-angle/

2 Milliken, William F & Milliken, Douglas L. 1995. Race Car Vehicle Dynamics. USA: Eleventh printing.

3 Asymmetric Tire Data and Optimum Tire. OptimumG. 2012. Available from: https://optimumg.com/asymmetric-tire-data-and-optimumtire/

4 Motorsports Tire Testing. Calspan. Available from: https://calspan.com/automotive/tire-performance-testing/motorsports-tire-testing

5 Pacejka, Hans. 2012. Tire and Vehicle Dynamics. Great Britain: Elsevier

6 Tire Model Selection. GCAPS. Available from: https://www.gcaps.net/2021/04/06/tire-model-selection/

7 Oikarinen, Pasi. Auton ajodynamiikka. Auton dynamiikka. Finland: Educational material, Metropolia University of Applied Sciences

8 Scrub Radius. Suspension Secrets. Available from: https://suspensionsecrets.co.uk/scrub-radius/

9 Segers, Jörge. 2008. Analysis Techniques for Racecar Data Acquisition. USA: SAE International.

10 Rules & Documents. Formula Student Germany. Available from: https://www.formulastudent.de/fsg/rules/

11 Jalali, Kiumars; Uchida, Thomas; McPhee, John & Lambert, Steve. 2013. SAE International Journal of Passenger Cars - Electronic and Electrical Systems. USA: SAE

Front Suspension Attachment Points

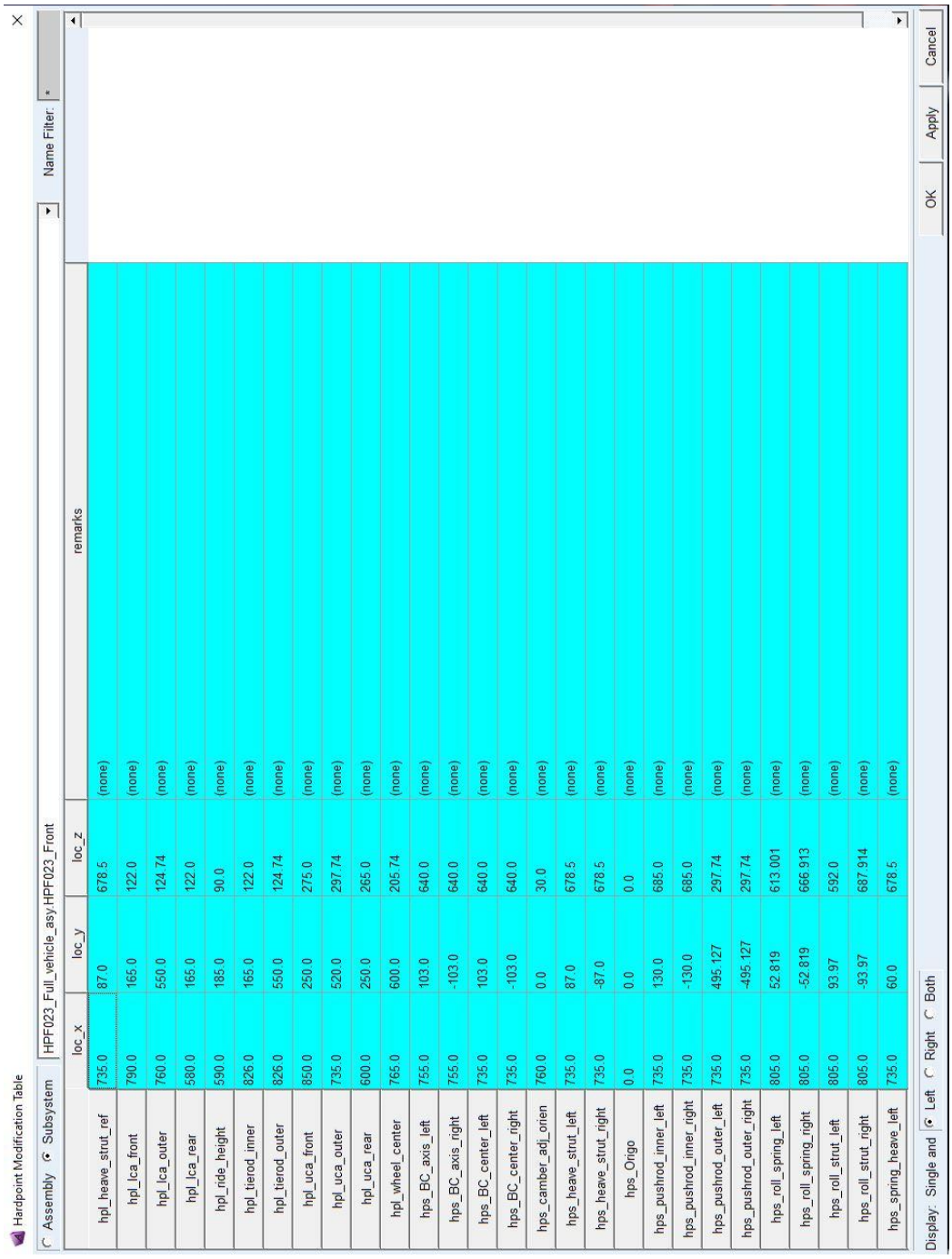

	loc_x	loc_y	loc_z	remarks
hpl_heave_strut_ref	735.0	87.0	678.5	(none)
hpl_lca_front	790.0	165.0	122.0	(none)
hpl_lca_outer	760.0	550.0	124.74	(none)
hpl_lca_rear	580.0	165.0	122.0	(none)
hpl_ride_height	590.0	185.0	90.0	(none)
hpl_tierod_inner	826.0	165.0	122.0	(none)
hpl_tierod_outer	826.0	550.0	124.74	(none)
hpl_uca_front	850.0	250.0	275.0	(none)
hpl_uca_outer	735.0	520.0	297.74	(none)
hpl_uca_rear	600.0	250.0	265.0	(none)
hpl_wheel_center	765.0	600.0	205.74	(none)
hps_BC_axis_left	755.0	103.0	640.0	(none)
hps_BC_axis_right	755.0	-103.0	640.0	(none)
hps_BC_center_left	735.0	103.0	640.0	(none)
hps_BC_center_right	735.0	-103.0	640.0	(none)
hps_camber_adj_orien	760.0	0.0	30.0	(none)
hps_heave_strut_left	735.0	87.0	678.5	(none)
hps_heave_strut_right	735.0	-87.0	678.5	(none)
hps_Origo	0.0	0.0	0.0	(none)
hps_pushrod_inner_left	735.0	130.0	685.0	(none)
hps_pushrod_inner_right	735.0	-130.0	685.0	(none)
hps_pushrod_outer_left	735.0	495.127	297.74	(none)
hps_pushrod_outer_right	735.0	-495.127	297.74	(none)
hps_roll_spring_left	805.0	52.819	613.001	(none)
hps_roll_spring_right	805.0	-52.819	666.913	(none)
hps_roll_strut_left	805.0	93.97	592.0	(none)
hps_roll_strut_right	805.0	-93.97	687.914	(none)
hps_spring_heave_left	735.0	60.0	678.5	(none)

Rear Suspension Attachment Points

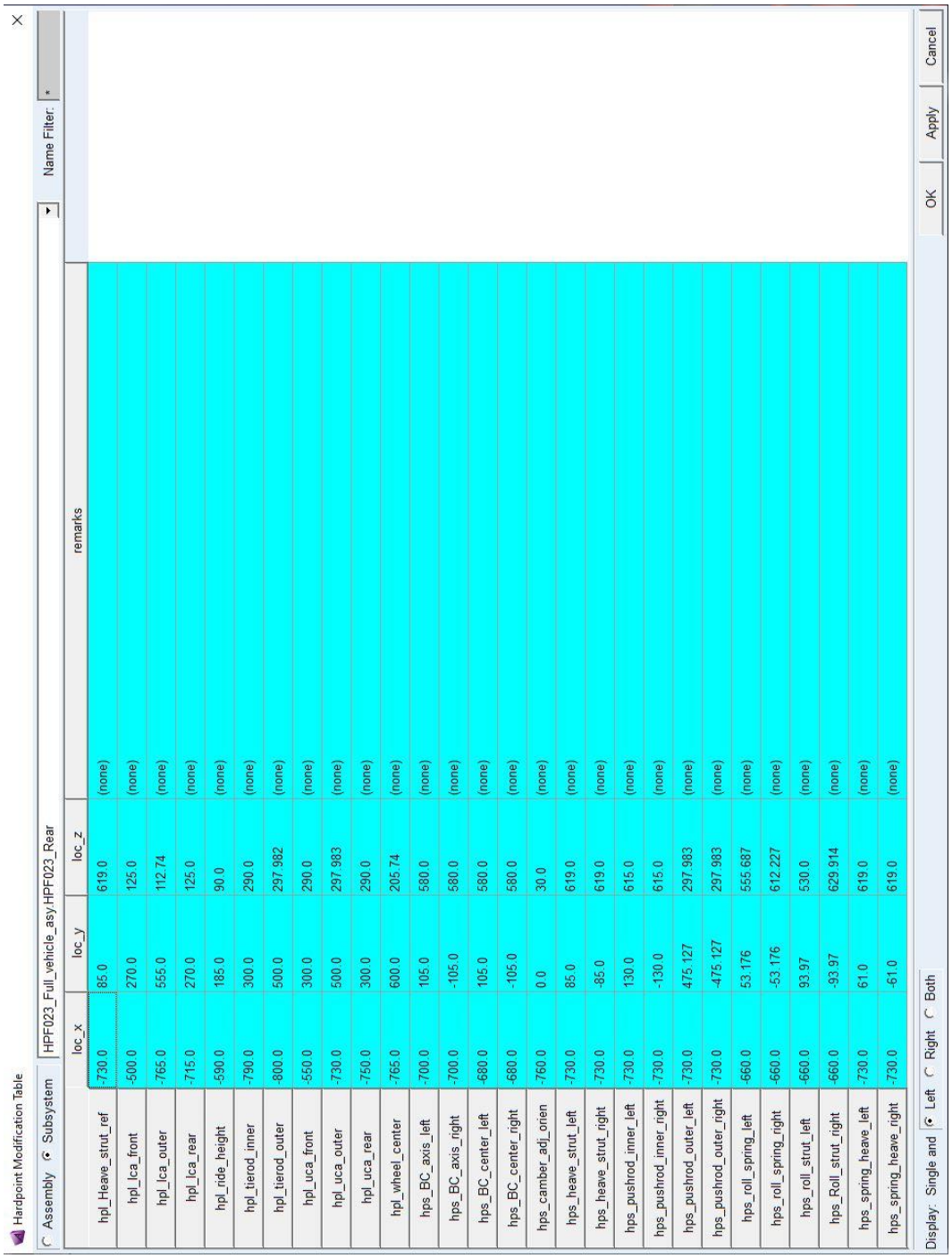

	loc_x	loc_y	loc_z	remarks
hpl_Heave_strut_ref	-730.0	85.0	619.0	(none)
hpl_lca_front	-500.0	270.0	125.0	(none)
hpl_lca_outer	-765.0	555.0	112.74	(none)
hpl_lca_rear	-715.0	270.0	125.0	(none)
hpl_ride_height	-590.0	185.0	90.0	(none)
hpl_tierod_inner	-790.0	300.0	290.0	(none)
hpl_tierod_outer	-800.0	500.0	297.982	(none)
hpl_uca_front	-550.0	300.0	290.0	(none)
hpl_uca_outer	-730.0	500.0	297.983	(none)
hpl_uca_rear	-750.0	300.0	290.0	(none)
hpl_wheel_center	-765.0	600.0	205.74	(none)
hps_BC_axis_left	-700.0	105.0	580.0	(none)
hps_BC_axis_right	-700.0	-105.0	580.0	(none)
hps_BC_center_left	-680.0	105.0	580.0	(none)
hps_BC_center_right	-680.0	-105.0	580.0	(none)
hps_camber_adj_orien	-760.0	0.0	30.0	(none)
hps_heave_strut_left	-730.0	85.0	619.0	(none)
hps_heave_strut_right	-730.0	-85.0	619.0	(none)
hps_pushrod_inner_left	-730.0	130.0	615.0	(none)
hps_pushrod_inner_right	-730.0	-130.0	615.0	(none)
hps_pushrod_outer_left	-730.0	475.127	297.983	(none)
hps_pushrod_outer_right	-730.0	-475.127	297.983	(none)
hps_roll_spring_left	-660.0	53.176	555.687	(none)
hps_roll_spring_right	-660.0	-53.176	612.227	(none)
hps_roll_strut_left	-660.0	93.97	530.0	(none)
hps_Roll_strut_right	-660.0	-93.97	629.914	(none)
hps_spring_heave_left	-730.0	61.0	619.0	(none)
hps_spring_heave_right	-730.0	-61.0	619.0	(none)

Steering Attachment Points

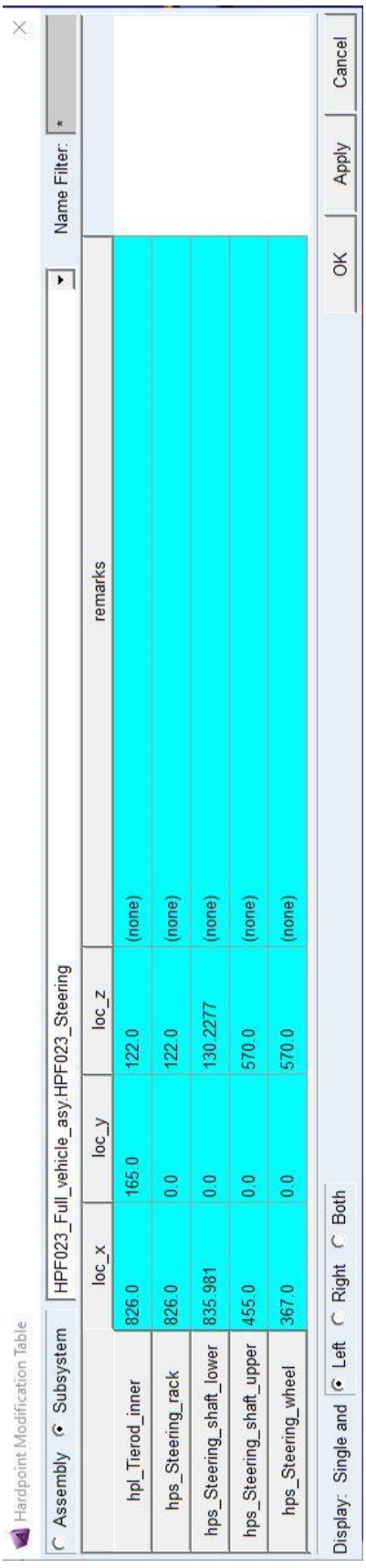

Chassis Attachment Points

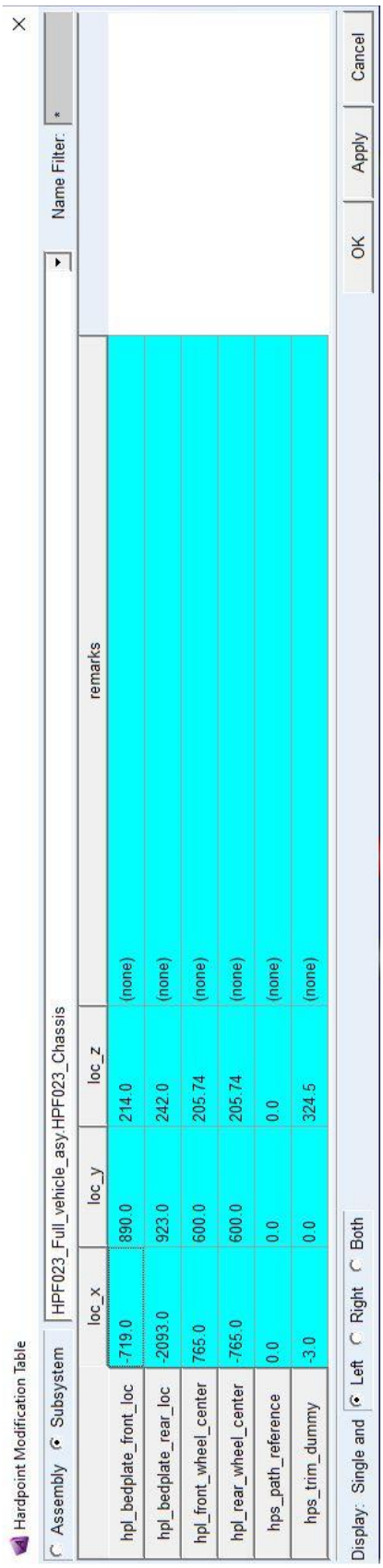

Topology of Connected Parts with Chassis in Full Vehicle Model

```
HPF023_Chassis.ges_chassis (Part) is connected to
    testrig.ges_gyro          via  testrig.gyro_body_hooke          (Hooke Joint)
    HPF023_Front.gel_lower_control_arm  via  HPF023_Front.jklrev_lca  (deactivated Revolute Joint)
    HPF023_Front.gel_lower_control_arm  via  HPF023_Front.bgl_lca_front.field  (Field)
    HPF023_Front.gel_lower_control_arm  via  HPF023_Front.bgl_lca_rear.field  (Field)
    HPF023_Front.ger_lower_control_arm  via  HPF023_Front.jkrrev_lca  (deactivated Revolute Joint)
    HPF023_Front.ger_lower_control_arm  via  HPF023_Front.bgr_lca_front.field  (Field)
    HPF023_Front.ger_lower_control_arm  via  HPF023_Front.bgr_lca_rear.field  (Field)
    HPF023_Front.gel_upper_control_arm  via  HPF023_Front.jklrev_uca  (deactivated Revolute Joint)
    HPF023_Front.gel_upper_control_arm  via  HPF023_Front.bgl_uca_front.field  (Field)
    HPF023_Front.gel_upper_control_arm  via  HPF023_Front.bgl_uca_rear.field  (Field)
    HPF023_Front.ger_upper_control_arm  via  HPF023_Front.jkrrev_uca  (deactivated Revolute Joint)
    HPF023_Front.ger_upper_control_arm  via  HPF023_Front.bgr_uca_front.field  (Field)
    HPF023_Front.ger_upper_control_arm  via  HPF023_Front.bgr_uca_rear.field  (Field)
    HPF023_Front.ges_BC_left  via  HPF023_Front.josrev_BC_center_left  (Revolute Joint)
    HPF023_Front.ges_BC_right  via  HPF023_Front.josrev_BC_center_right  (Revolute Joint)
    HPF023_Rear.gel_lower_control_arm  via  HPF023_Rear.jklrev_lca  (Revolute Joint)
    HPF023_Rear.gel_lower_control_arm  via  HPF023_Rear.bgl_lca_front.field  (deactivated Field)
    HPF023_Rear.gel_lower_control_arm  via  HPF023_Rear.bgl_lca_rear.field  (deactivated Field)
    HPF023_Rear.ger_lower_control_arm  via  HPF023_Rear.jkrrev_lca  (Revolute Joint)
    HPF023_Rear.ger_lower_control_arm  via  HPF023_Rear.bgr_lca_front.field  (deactivated Field)
    HPF023_Rear.ger_lower_control_arm  via  HPF023_Rear.bgr_lca_rear.field  (deactivated Field)
    HPF023_Rear.gel_upper_control_arm  via  HPF023_Rear.jklrev_uca  (Revolute Joint)
    HPF023_Rear.gel_upper_control_arm  via  HPF023_Rear.bgl_uca_front.field  (deactivated Field)
    HPF023_Rear.gel_upper_control_arm  via  HPF023_Rear.bgl_uca_rear.field  (deactivated Field)
    HPF023_Rear.ger_upper_control_arm  via  HPF023_Rear.jkrrev_uca  (Revolute Joint)
    HPF023_Rear.ger_upper_control_arm  via  HPF023_Rear.bgr_uca_front.field  (deactivated Field)
    HPF023_Rear.ger_upper_control_arm  via  HPF023_Rear.bgr_uca_rear.field  (deactivated Field)
    HPF023_Rear.ges_BC_left  via  HPF023_Rear.josrev_BC_center_left  (Revolute Joint)
    HPF023_Rear.ges_BC_right  via  HPF023_Rear.josrev_BC_center_right  (Revolute Joint)
    HPF023_Rear.gel_tierod_inner  via  HPF023_Rear.jolcon_tierod_inner  (Convel Joint)
    HPF023_Rear.ger_tierod_inner  via  HPF023_Rear.jorcon_tierod_inner  (Convel Joint)
    HPF023_Steering.ges_Steering_rack  via  HPF023_Steering.jostra_Steering_rack_movement  (Translational Joint)
    HPF023_Steering.ges_Steering_wheel  via  HPF023_Steering.josrev_Steering_wheel_movement  (Revolute Joint)
    HPF023_Steering.ges_Pinion  via  HPF023_Steering.josrev_Pinion_revolute  (Revolute Joint)
    HPF023_Steering.ges_Angle_gear_shaft  via  HPF023_Steering.josrev_Angle_gear_shaft_movement  (Revolute Joint)
    HPF023_Steering.ges_Steering_shaft  via  HPF023_Steering.josrev_Steering_shaft_movement  (Revolute Joint)
    HPF023_Chassis.ges_trim_mass  via  HPF023_Chassis.josfix_trim_mass  (Fixed Joint)
    testrig.ground            via  testrig.josinl_body_stake        (Inline Primitive_Joint)
    testrig.ground            via  testrig.josper_yaw_stake         (Perpendicular Primitive_Joint)
    testrig.ground            via  testrig.sse_mmm_motion           (deactivated Point Motion)
    HPF023_Chassis.ground     via  HPF023_Chassis.aero_forces       (General_Force)
```

Hoosier LC0 Tire Model

```
[MDI_HEADER]
FILE_TYPE                ='tir'
FILE_VERSION             =3.0
FILE_FORMAT              ='ASCII'
! : TIRE_VERSION :      PAC2002
! : COMMENT :           Tire                    Lc0
! : COMMENT :           Manufacturer
! : COMMENT :           Nom. section width  (m)  0.19
! : COMMENT :           Nom. aspect ratio  (-)  0.4
! : COMMENT :           Infl. pressure    (Pa)  80000
! : COMMENT :           Rim diameter    (inch)  10
! : COMMENT :           Measurement ID
! : COMMENT :           Test speed       (m/s)  11.176
! : COMMENT :           Road surface
! : COMMENT :           Road condition          Dry
! : FILE_FORMAT :       ASCII
! : Copyright (C) 2004-2011 MSC Software Corporation
!
! USE_MODE specifies the type of calculation performed:
!       0: Fz only, no Magic Formula evaluation
!       1: Fx,My only
!       2: Fy,Mx,Mz only
!       3: Fx,Fy,Mx,My,Mz uncombined force/moment calculation
!       4: Fx,Fy,Mx,My,Mz combined force/moment calculation
!     +10: including relaxation behaviour
!     *-1: mirroring of tyre characteristics
!
!    example: USE_MODE = -12 implies:
!       -calculation of Fy,Mx,Mz only
!       -including relaxation effects
!       -mirrored tyre characteristics
!
$----------------------------------------------------------------units
[UNITS]
LENGTH                   ='meter'
FORCE                    ='newton'
ANGLE                    ='radian'
MASS                     ='kg'
TIME                     ='second'
$----------------------------------------------------------------model
[MODEL]
PROPERTY_FILE_FORMAT     ='PAC2002'
USE_MODE                 = 4                 $Tyre use switch (IUSED)
VXLOW                    = 1
LONGVL                   = 11.176              $Measurement speed
TYRESIDE                 = 'LEFT'             $Mounted side of tyre at vehicle/test bench
! 3D contact can be switched on by deleting the comment ! character
! When no further coefficients are specified, default values will be taken
!CONTACT_MODEL            = '3D_ENVELOPING'
$-------------------------------------------------------------dimensions
[DIMENSION]
UNLOADED_RADIUS          = 0.2047             $Free tyre radius
WIDTH                    = 0.19              $Nominal section width of the tyre
ASPECT_RATIO             = 0.40               $Nominal aspect ratio
RIM_RADIUS               = 0.127              $Nominal rim radius
RIM_WIDTH                = 0.2032             $Rim width
```

```
$----------------------------------------------------------------shape
[SHAPE]
{radial width}
 1.0    0.0
 1.0    0.4
 1.0    0.9
 0.9    1.0
$------------------------------------------------------------parameter
[VERTICAL]
VERTICAL_STIFFNESS       = 91766               $Tyre vertical stiffness
VERTICAL_DAMPING         = 112.452                  $Tyre vertical damping
BREFF                    = 1                 $Low load stiffness e.r.r.
DREFF                    = 1                $Peak value of e.r.r.
FREFF                    = 1.0001                $High load stiffness e.r.r.
FNOMIN                   = 657                $Nominal wheel load
$-----------------------------------------------------long_slip_range
[LONG_SLIP_RANGE]
KPUMIN                   = -0.15                $Minimum valid wheel slip
KPUMAX                   = 0.15                 $Maximum valid wheel slip
$---------------------------------------------------slip_angle_range
[SLIP_ANGLE_RANGE]
ALPMIN                   = -0.261799             $Minimum valid slip angle
ALPMAX                   = 0.261799              $Maximum valid slip angle
$-------------------------------------------inclination_slip_range
[INCLINATION_ANGLE_RANGE]
CAMMIN                   = -0.069813             $Minimum valid camber angle
CAMMAX                   = 0.069813              $Maximum valid camber angle
$-----------------------------------------------vertical_force_range
[VERTICAL_FORCE_RANGE]
FZMIN                    = 100                  $Minimum allowed wheel load
FZMAX                    = 1092                 $Maximum allowed wheel load
```

```
$-------------------------------------------------------------scaling
[SCALING_COEFFICIENTS]
LFZO                    = 1                  $Scale factor of nominal (rated) load
LCX                     = 1                  $Scale factor of Fx shape factor
LMUX                    = 1                  $Scale factor of Fx peak friction coefficient
LEX                     = 1                  $Scale factor of Fx curvature factor
LKX                     = 1                  $Scale factor of Fx slip stiffness
LHX                     = 1                  $Scale factor of Fx horizontal shift
LVX                     = 1                  $Scale factor of Fx vertical shift
LGAX                    = 1                  $Scale factor of camber for Fx
LCY                     = 1                  $Scale factor of Fy shape factor
LMUY                    = 1                  $Scale factor of Fy peak friction coefficient
LEY                     = 1                  $Scale factor of Fy curvature factor
LKY                     = 1                  $Scale factor of Fy cornering stiffness
LHY                     = 1                  $Scale factor of Fy horizontal shift
LVY                     = 1                  $Scale factor of Fy vertical shift
LGAY                    = 1                  $Scale factor of camber for Fy
LTR                     = 1                  $Scale factor of Peak of pneumatic trail
LRES                    = 1                  $Scale factor for offset of residual torque
LGAZ                    = 1                  $Scale factor of camber for Mz
LXAL                    = 1                  $Scale factor of alpha influence on Fx
LYKA                    = 1                  $Scale factor of alpha influence on Fx
LVYKA                   = 1                  $Scale factor of kappa induced Fy
LS                      = 1                  $Scale factor of Moment arm of Fx
LSGKP                   = 1                  $Scale factor of Relaxation length of Fx
LSGAL                   = 1                  $Scale factor of Relaxation length of Fy
LGYR                    = 1                  $Scale factor of gyroscopic torque
LMX                     = 1                  $Scale factor of overturning couple
LVMX                    = 1                  $Scale factor of Mx vertical shift
LMY                     = 1                  $Scale factor of rolling resistance torque
$-----------------------------------------------------------longitudinal
[LONGITUDINAL_COEFFICIENTS]
PCX1                    = 0.839797             $Shape factor Cfx for longitudinal force
PDX1                    = 2.61997             $Longitudinal friction Mux at Fznom
PDX2                    = -0.0599727           $Variation of friction Mux with load
PDX3                    = 5.38753        $Variation of friction Mux with camber
PEX1                    = -0.159988            $Longitudinal curvature Efx at Fznom
PEX2                    = -0.846665           $Variation of curvature Efx with load
PEX3                    = -0.186677           $Variation of curvature Efx with load squared
PEX4                    = -1         $Factor in curvature Efx while driving
PKX1                    = 52.0015             $Longitudinal slip stiffness Kfx/Fz at Fznom
PKX2                    = -25.4292             $Variation of slip stiffness Kfx/Fz with load
PKX3                    = 0.254987            $Exponent in slip stiffness Kfx/Fz with load
PHX1                    = -0.000755758        $Horizontal shift Shx at Fznom
PHX2                    = 0.00195599        $Variation of shift Shx with load
PVX1                    = 0.0490469         $Vertical shift Svx/Fz at Fznom
PVX2                    = -0.158215         $Variation of shift Svx/Fz with load
RBX1                    = 169.575             $Slope factor for combined slip Fx reduction
RBX2                    = 82.5226            $Variation of slope Fx reduction with kappa
RCX1                    = 0.940506             $Shape factor for combined slip Fx reduction
REX1                    = 0.545493              $Curvature factor of combined Fx
REX2                    = 0.216          $Curvature factor of combined Fx with load
RHX1                    = -0.0165874           $Shift factor for combined slip Fx reduction
PTX1                    = 0               $Relaxation length SigKap0/Fz at Fznom
PTX2                    = 0            $Variation of SigKap0/Fz with load
PTX3                    = 0               $Variation of SigKap0/Fz with exponent of load
```

```
$------------------------------------------------------------overturning
[OVERTURNING_COEFFICIENTS]
QSX1                    = -0.0300152                 $Lateral force induced overturning moment
QSX2                    = -0.882267                 $Camber induced overturning couple
QSX3                    = 0.0513197                 $Fy induced overturning couple
$-------------------------------------------------------------------lateral
[LATERAL_COEFFICIENTS]
PCY1                    = 1.38875              $Shape factor Cfy for lateral forces
PDY1                    = -2.28868              $Lateral friction Muy
PDY2                    = 0.31465            $Variation of friction Muy with load
PDY3                    = 7.595             $Variation of friction Muy with squared camber
PEY1                    = -0.0101673            $Lateral curvature Efy at Fznom
PEY2                    = -0.0451511           $Variation of curvature Efy with load
PEY3                    = 0.279605            $Zero order camber dependency of curvature Efy
PEY4                    = -0.228768             $Variation of curvature Efy with camber
PKY1                    = -60.9384             $Maximum value of stiffness Kfy/Fznom
PKY2                    = 3.26168              $Load at which Kfy reaches maximum value
PKY3                    = 1.13736           $Variation of Kfy/Fznom with camber
PHY1                    = -3.81992e-05           $Horizontal shift Shy at Fznom
PHY2                    = 0.00226296        $Variation of shift Shy with load
PHY3                    = 0.170933            $Variation of shift Shy with camber
PVY1                    = 0.0535199            $Vertical shift in Svy/Fz at Fznom
PVY2                    = 0.0135882          $Variation of shift Svy/Fz with load
PVY3                    = 1.81785           $Variation of shift Svy/Fz with camber
PVY4                    = -1.35235            $Variation of shift Svy/Fz with camber and load
RBY1                    = 15.4              $Slope factor for combined Fy reduction
RBY2                    = 5.6              $Variation of slope Fy reduction with alpha
RBY3                    = -0.0480804            $Shift term for alpha in slope Fy reduction
RCY1                    = 0.834114             $Shape factor for combined Fy reduction
REY1                    = 0.3            $Curvature factor of combined Fy
REY2                    = -0.120613          $Curvature factor of combined Fy with load
RHY1                    = 0.00315489          $Shift factor for combined Fy reduction
RHY2                    = 0.00372705         $Shift factor for combined Fy reduction with load
RVY1                    = 0.00646275            $Kappa induced side force Svyk/Muy*Fz at Fznom
RVY2                    = 0.00296026           $Variation of Svyk/Muy*Fz with load
RVY3                    = -0.0887685           $Variation of Svyk/Muy*Fz with camber
RVY4                    = -50               $Variation of Svyk/Muy*Fz with alpha
RVY5                    = -3                  $Variation of Svyk/Muy*Fz with kappa
RVY6                    = 22                    $Variation of Svyk/Muy*Fz with atan(kappa)
PTY1                    = 0                 $Peak value of relaxation length SigAlp0/R0
PTY2                    = 0                $Value of Fz/Fznom where SigAlp0 is extreme
$-----------------------------------------------------rolling resistance
[ROLLING_COEFFICIENTS]
QSY1                    = 0                $Rolling resistance torque coefficient
QSY2                    = 0                   $Rolling resistance torque depending on Fx
QSY3                    = 0                   $Rolling resistance torque depending on speed
QSY4                    = 0                   $Rolling resistance torque depending on speed ^4
```

```
$------------------------------------------------------------aligning
[ALIGNING_COEFFICIENTS]
QBZ1                    = 8.19543             $Trail slope factor for trail Bpt at Fznom
QBZ2                    = 1.96922            $Variation of slope Bpt with load
QBZ3                    = -4.77067            $Variation of slope Bpt with load squared
QBZ4                    = -0.429117            $Variation of slope Bpt with camber
QBZ5                    = 0.792014            $Variation of slope Bpt with absolute camber
QBZ9                    = 0             $Slope factor Br of residual torque Mzr
QBZ10                   = -1.7778                $Slope factor Br of residual torque Mzr
QCZ1                    = 1.4192             $Shape factor Cpt for pneumatic trail
QDZ1                    = 0.146159           $Peak trail Dpt" = Dpt*(Fz/Fznom*R0)
QDZ2                    = -0.0552863         $Variation of peak Dpt" with load
QDZ3                    = 0.387762           $Variation of peak Dpt" with camber
QDZ4                    = -3.95699              $Variation of peak Dpt" with camber squared
QDZ6                    = 0.0109099          $Peak residual torque Dmr" = Dmr/(Fz*R0)
QDZ7                    = -0.00313689           $Variation of peak factor Dmr" with load
QDZ8                    = -2.02785           $Variation of peak factor Dmr" with camber
QDZ9                    = -0.190885           $Variation of peak factor Dmr" with camber and load
QEZ1                    = -0.228768            $Trail curvature Ept at Fznom
QEZ2                    = 1.23699             $Variation of curvature Ept with load
QEZ3                    = -1.88318                 $Variation of curvature Ept with load squared
QEZ4                    = 0             $Variation of curvature Ept with sign of Alpha-t
QEZ5                    = 0.244             $Variation of Ept with camber and sign Alpha-t
QHZ1                    = 0.000581082         $Trail horizontal shift Sht at Fznom
QHZ2                    = -0.00196897           $Variation of shift Sht with load
QHZ3                    = -0.0247388            $Variation of shift Sht with camber
QHZ4                    = 0.00806322            $Variation of shift Sht with camber and load
SSZ1                    = -0.0778385           $Nominal value of s/R0: effect of Fx on Mz
SSZ2                    = -0.0393202           $Variation of distance s/R0 with Fy/Fznom
SSZ3                    = 1.62473            $Variation of distance s/R0 with camber
SSZ4                    = -0.65957            $Variation of distance s/R0 with load and camber
QTZ1                    = 0                  $Gyration torque constant
MBELT                   = 0                  $Belt mass of the wheel
```